Mucus production, host-microbiome interactions, hormone sensitivity, and innate immune responses modeled in human endo- and ecto-cervix chips

Zohreh Izadifar[1], Justin Cotton[1], Cathy Chen[2], Nicole A. Bustos[3], Viktor Horvath[1], Anna Stejskalova[1], Chloe Wu[4], Aakanksha Gulati[1], Nina T. LoGrande[1], Erin Dohetry[1], Tania To[1], Sarah E. Gilpin[1], Adama M. Sesay[1], Girija Goyal[1], Katharina Ribbeck[4], Carlito Lebrilla[2], and Donald E. Ingber[1,5*]

[1]Wyss Institute for Biologically Inspired Engineering, Harvard University, Boston, MA 02115

[2]Department of Chemistry, University of California Davis, Davis, California, CA 95616

[3]Department of Mechanical Engineering, Massachusetts Institute of Technology, Cambridge, MA 02139

[4]Department of Biological Engineering, Massachusetts Institute of Technology, Cambridge, MA 02141

[5]Vascular Biology Program, Boston Children's Hospital and Department of Pathology, Harvard Medical School, Boston, MA 02115

[*]Address all correspondence to: don.ingber@wyss.harvard.edu

---

ABSTRACT

Modulation of mucus production by the human ecto- and endo-cervical epithelium by steroid hormones and associated interactions with commensal microbiome play a central role in the physiology and pathophysiology of the female reproductive tract. However, most of our knowledge about these interactions is based on results from animal studies or *in vitro* models that fail to faithfully mimic the mucosal environment of the human cervix. Here we describe microfluidic organ-on-a-chip (Organ Chip) models of the human cervical mucosa that recreate the cervical epithelial-stromal interface with a functional epithelial barrier and produce abundant mucus that has compositional, biophysical, and

hormone-responsive properties similar to the living cervix. Use of continuous fluid flow promoted ecto-cervical differentiation, whereas use of periodic flow including periods of stasis stimulated endo-cervical specialization. Similar results with minor differences were obtained using epithelial cells isolated from three donors each from a different ethnic background (African American, Hispanic, and Caucasian). When the endo-Cervix Chips were co-cultured with living *Lactobacillus crispatus* and *Gardnerella vaginalis* bacterial communities to respectively mimic the effects of human host interactions with optimal (healthy) or non-optimal (dysbiotic) microbiome, significant differences in tissue innate immune responses, barrier function, cell viability, and mucus composition were detected reminiscent of those observed *in vivo*. Thus, human Cervix Chips provide a physiologically relevant experimental *in vitro* model to study cervical mucus physiology and its role in human host-microbiome interactions as well as a potential preclinical testbed for development of therapeutic interventions to enhance women's health.

INTRODUCTION

In most women, the optimal healthy state of the lower reproductive tract is characterized by a symbiotic relationship with a cervico-vaginal microbiome composed of a stable community of bacteria dominated by *Lactobacillus crispatus* [1]. When a dysbiotic state develops, such as bacterial vaginosis (BV), this composition shifts and the *L. crispatus* community is replaced by a non-stable community of diverse 'non-optimal' anaerobes with an increased presence of more pathogenic bacteria, such as *Gardnerella vaginalis* and fewer *L. crispatus* [2]. BV is a common clinical condition that affects > 25% of reproductive-age women globally [3] and contributes to significant adverse health outcomes including increased risk of acquiring human immunodeficiency virus (HIV) and other sexually transmitted infections [4,5] as well as higher rates of spontaneous abortion, pre-term birth, miscarriage, low birth weight, pelvic inflammatory disease, and postpartum endometritis [6-8]. Current therapeutic options include antimicrobial and probiotic regimens and biofilm disruption [2], however, they are of limited value

and have a high failure rate that results in frequent recurrence (up to 50% within one year) [9]. Although the BV syndrome was first described over a century ago, the mechanisms that underlie this condition and the casual linkages between dysbiosis and adverse health outcomes still remain unknown, which has prevented development of more effective treatment and prevention strategies [3,10]. This is in part because most of our current knowledge and therapeutic development approaches are based on results of studies of microbial cultures [11,12], metagenomic analyses [1,13,14], or *in vitro* models [10] that fail to faithfully mimic the complex tissue microenvironment of the human reproductive tract.

The mucus layer that lines the epithelial surfaces of the reproductive tract is increasingly recognized as a key contributor to fertility and pregnancy, as well as reproductive and genital health outcomes [15-17], although the underlying mechanisms remain poorly understood. This mucus layer is primarily produced and secreted by the epithelium lining the endo- and ecto-cervix and its structure, composition and physiological features change dramatically with hormonal (e.g., sex steroids) and environmental (i.e. pH, oxygen tension) alterations. Changes in bacterial composition also can reciprocally stimulate host transcriptional and immune responses[18-21], thereby further altering mucus composition as well as the associated vagino-cervical microbiome [14]. For instance, changes in sex hormone levels during menarche, menses, pregnancy and menopause alter both the vaginal microbiome [22,23] and mucus properties [24,25]; however, it is currently impossible to determine whether these changes in mucus alter the microbiome or vice versa *in vivo* in the human cervix. Little is also known about differences between endo- and ecto-cervical physiology. Thus, to tease out the dynamic interactions between different contributing factors and thereby, potentially provide new approaches to reduce the burden of BV and its associated health and economic sequelae among millions of women around the world, it would be helpful to have an *in vitro* model of the human cervical mucosa that can recapitulate the physiology and complexity of these different cervical microenvironments yet allow for

controlled perturbation and analysis of how these various potential contributors influence reproductive health and disease.

Although current *in vitro* culture systems, such as two dimensional (2D) planar cultures [26,27], Transwell inserts with porous membranes [14,28], and three dimensional (3D) engineered constructs [18,29,30], have been used to study cervical epithelial cell interactions with bacteria and microbicides as well as innate immune responses [26,27], they fail to recapitulate the tissue-tissue interfaces, barrier properties, mucus production, or molecular signaling and secretory profile dynamics that are observed in human cervix *in vivo* . In particular, the cervical mucus that plays such a key role in maintaining healthy host-microbiome interactions has not been modeled effectively *in vitro*. It is equally difficult to study interactions between human cervical epithelium with living microbiome for extended times (> 1 day) in these static cultures because the microbes overgrow and kill the human cells. Because of these limitations, existing models of the human cervix cannot be used to analyze complex host-microbiome interactions that are observed *in vivo* for meaningful preclinical screening of new therapeutics and other clinical interventions.

Importantly, organ-on-chip (Organ Chip) microfluidic culture technology that enables investigators to recreate organ-level structures including tissue-tissue interfaces that experience dynamic fluid flow *in vitro* offers a potential way to overcome these challenges [31,32]. In fact, we recently described a human Vagina Chip lined by primary human vaginal epithelium and underlying stromal fibroblasts that faithfully recapitulates the structure and function of the human vaginal mucosa [33]. However, as the cervix is a major source of the mucus that normally serves as a protective covering over the surface of the cervical and vaginal epithelium that interacts directly with resident bacterial flora in the entire lower female reproductive tract [17,34,35], we extended this approach here to develop an Organ Chip model of the human cervical mucosa (Cervix Chip) lined by primary human cervical epithelium interfaced with human cervical stromal fibroblasts.

The ectocervix and endocervix that open into the vagina and lead into the uterus, respectively, are lined by an epithelium that forms a tight tissue barrier and spontaneously produces an overlying cervical mucus layer *in vivo*. By culturing a mixture of primary human endo- and ecto-cervical epithelial cells, interfacing them with cervical fibroblasts, and culturing them under different dynamic flow conditions on-chip, we were able to create Cervix Chips that preferentially express an ecto- or endo-cervical phenotype and which respond to hormonal, environmental, and microbial cues in a manner similar to that observed *in vivo*.

RESULTS

Engineering of mucus-producing human Organ Chip models of endo- and ecto-cervix

Organ Chip models of the human cervical mucosa were developed using a commercially available microfluidic chip (Emulate Inc., Boston MA) composed of an optically clear silicone rubber polymer that contains two microchannels separated by a thin, porous membrane of the same material (**Fig. 1a**). To recreate the human cervical epithelial-stromal interface on-chip, a commercially available mixture of primary human endo- and ecto-cervical epithelial cells (**Supplementary Fig. S1a**) were cultured on the top surface of the porous membrane which was pre-coated with extracellular matrix (ECM) and primary human cervical stromal fibroblasts isolated from healthy cervical tissue were cultured on the lower surface of the same membrane (**Fig. 1a,b**). Because the optimal flow condition necessary to support epithelial cell differentiation and mucus production on-chip was not known, two different flow regimens were tested: continuous perfusion of the upper channel with epithelial growth medium (Continuous) or intermittent perfusion in which the same medium was flowed for 4 hrs followed by 20 hours of static culture (Periodic) to mimic periodic mucus flow that can occur *in vivo*. In both conditions, the lower channels were perfused continuously with stromal growth medium. After 5 days, the apical medium was replaced with a customized Hank's Buffer Saline Solution (HBSS) at pH ~5.4 with lower buffer salts and no glucose (LB/-G) to simulate the slightly acidic pH of the cervix [36], while the

stromal growth medium was replaced with differentiation medium containing the female sex hormone estradiol-17β (E2) at a dose (5 nM) that represents the peak estrogen level experienced during the ovulatory phase of the menstrual cycle [37].

Both cell types formed confluent monolayers within 1 day after seeding, and dark amorphous regions of what appeared to be mucus accumulation were detected above the epithelium when viewed from above by phase contrast microscopy (**Fig. 1b**). Similarly, when viewed from the side by dark field microscopic imaging of live cultured chips (which allows direct visualization of mucus on-chip)[31] after 7 days of differentiation (culture day 12), a fuzzy, white, light scattering material had accumulated above the epithelium nearly filling the apical channel (**Fig. 1c**). This was observed using both continuous and periodic flow regimens and the material stained positively with fluorescently labeled Wheat Germ Agglutinin (WGA) lectin, which preferentially binds to the glycans of the major MUC5B mucus protein[38] (**Fig. 1c,d**). This was further validated using immunofluorescence microscopic imaging of chips stained for MUC5B and F-actin which confirmed the presence of this primary gel-forming mucin type of human cervical mucus[34,39] within the cervical epithelial cells when viewed from above (**Fig. 1e**) or from the side in vertical cross sections (**Fig. 1f**). This latter study also confirmed the presence of vimentin-containing fibroblasts on the underside of the membrane (**Fig. 1f**) as well as expression of cytokeratin 18 (CK18), estrogen receptor (ER), and progesterone receptor (PGR) in the cervical epithelial cells (**Supplementary Fig. S1b**), which mimics their expression observed in the cervix *in vivo* [40].

Quantification of mucus accumulation using a colorimetric Alcian Blue assay [41] confirmed that there was a significant (~3-fold) increase in the total amount of mucin after 7 days of differentiation on chip under both continuous and period flow conditions (**Fig. 1g**). Quantitative analysis of immunofluorescence images of vertical cross-sections of continuous culture chips stained for MUC5B independently showed a similar 3-fold increase in the epithelial surface area covered by MUC5B-containing mucus secretions and this was accompanied by a concomitant decline in cell proliferation as

measured by decreased expression of the proliferation marker Ki67 (from ~60% to <10% labeling index) over the more than week-long differentiation time course (**Supplementary Fig. S1c**). Real time quantitative PCR (RT-qPCR) of the differentiated epithelial cells also demonstrated significant upregulation of genes encoding MUC5B as well as MUC4 and secretory leukocyte peptidase inhibitor (SLPI) at day 7 of differentiation on-chip compared to when the same cells were cultured in conventional 2D cultures using the same medium where these genes were barely expressed (**Supplementary Fig. S1d**).

Importantly, reconstitution of this epithelial-stromal interface similar to that observed *in vivo* was accompanied by establishment of a stable tissue barrier, as demonstrated by measuring real-time transepithelial electrical resistance (TEER) using electrodes that were integrated into custom made Organ Chips of the same design and composition, which enable continuous and quantitative measurement of barrier function over many days in culture[42]. The cervical mucosa formed on-chip maintained a barrier with high electrical resistance ranging from 2,700-26,000 ohm (Ω), which was significantly greater than that generated when the same cells were cultured under static conditions in a commercial Transwell insert using the same medium conditions (**Supplementary Fig. S1e**). In both the chip and Transwell models, the cervical tissue barrier maintained higher levels of TEER during the expansion phase and the first 2 days of differentiation, which then decreased and stabilized at a lower level, as previously observed in other *in vitro* epithelial models (e.g., lung airway) [43].

We then analyzed the innate immune status of these Cervix Chips by quantifying cytokine protein levels in the effluents of the upper epithelial channels, which revealed that the induction of epithelial cell differentiation and mucus accumulation at day 7 of differentiation was accompanied by a significant reduction in the levels of the pro-inflammatory cytokines. IL-1α, IL-1β, and IL-6 levels decreased regardless of whether cells were cultured under continuous or periodic flow; however,

exposure to continuous flow reduced IL-8 and TNF-α levels as well whereas chips exposed to periodic flow did not (**Fig. 1h**).

Interestingly, when we carried out RNA seq analysis of the cervical epithelium under the different flow conditions on-chip, we found that cells cultured under continuous flow exhibited significant upregulation of genes associated with ectocervical epithelial phenotype [44] whereas the same cells cultured in the same medium under periodic flow or under static conditions in Transwell inserts upregulated genes more closely associated with the endocervical epithelial phenotype[44] (**Fig. 1i**). As the primary cells we used contain a mixture of both endo- and ecto-cervical cells, these different flow conditions likely either promote growth and differentiation of a different subclass of cervical epithelial cells or they have differential effects on cervical epithelial cell specialization. This finding that exposure to continuous flow results in preferential expression of the ectocervical phenotype compared to periodic flow which exhibited more endocervical features was confirmed in three different human donors, each with a different ethnic background (Caucasian, Afro-American, or Hispanic) using a gene set scoring analysis method [45] (**Supplementary Fig. S1f**). Interestingly, cells from the Afro-American and Caucasian donors behaved differently when cultured in static Transwells where they expressed significantly more endocervical features even compared with periodic flow that also experienced intermittent static periods, while the Hispanic cells in Transwell behaved similarly to the periodic flow chip. However, while the Caucasian chips cultured under continuous flow did exhibit a more ectocervical gene expression profile compared to when it was in a Transwell, the continuous flow chips lined by cells from the other two donors more closely resembled the ectocervical phenotype observed *in vivo* (**Supplementary Fig. S1f**).

While it is too preliminary to ascribe ethnicity-dependencies to these responses given the low number of donors, these results suggests that the continuous flow condition preferentially promotes ecto-cervical differentiation, while periodic flow that includes static periods and conventional Transwell

cultures promote endo-cervical specialization. However, it is important to note that the Cervix Chip phenotype under periodic flow is distinct from that displayed by the same cells in the same medium in static Transwells. For example, while MUC5B appears to be expressed at a similar level under both conditions, MUC4 gene expression in the cervical epithelium was significantly higher on-chip (**Supplementary Fig. S1d**). Cervix Chips cultured under periodic flow also exhibited enhanced epithelial barrier integrity compared to Transwells (**Supplementary Fig. S1e**). There were also differences in the cell morphology in Transwells versus chips with the epithelium forming a more regular polygonal cell layer and the stroma exhibiting greater alignment in the Cervix Chip cultured under periodic flow (**Supplementary Fig. S1g**).

Analysis of cervical mucus chemistry, biophysics, and physiology on-chip

Mucin proteins are heavily glycosylated (40-80%) and their composition and glycomic structure play an important role in fundamental inter- and intra-cellular processes and immune modulation functions of the cervix[46,47]. To characterize the biochemical composition of the Cervix Chip mucus, structural glycomics analysis of the O- and N-linked glycans of the mucin glycoproteins was performed. O- and N-glycans were first released and then individually profiled using Agilent nanoscale liquid chromatography quadrupole time-of-flight coupled to tandem mass spectrometry (nanoLC-QTOF MS/MS)[46]. The mucus isolated from the epithelial channel of the Cervix Chip contained >50 O- and 350 N-glycans and >11 O- and 129 N-glycans when cultured under continuous and periodic flow, respectively, with the undecorated, sialylated, sialofucosylated, and fucosylated glycan components being the most abundant molecular species identified. Comparison of the O- and N-glycosylation profiles of mucus isolated from Cervix Chips cultured under periodic versus continuous flow revealed that more diverse O- and N-glycan structures were observed in the mucus from the continuous flow chip (**Fig. 2a**). However, some of the most abundant glycan structures, including sialylated O-glycans (2_2_0_2|28.2), (2_2_0_1|23.5), (3_3_0_2|30.2), (3_3_0_2|31.3) and sialylated N-glycans (5_4_0_2|27.5) and

sialofucosylated (5_4_1_1|25.3), were detected in both chips. Interestingly, higher levels of O-glycans were detected in mucus from the periodic flow chips, whereas an opposite trend was observed for the N-glycans. For example, based on ions counts and area under the curve the sialylated O-glycans (2_2_0_2|28.2) were >6-fold higher in mucus of periodic flow chip compared to chips exposed to continuous flow, while the sialylated N-glycan (5_4_0_2|27.5) was >7-fold higher in continuous flow chips (**Fig. 2a**). In other words, the endo-cervical chips preferentially produce a mucus dominated by O-glycans, while the ecto-cervical chips predominantly produce N-glycans. When we compared O- and N-glycan profiles of mucus isolated from these Cervix Chips with those produced by cells in Transwell culture, we found they were distinct in that the Transwells failed to produce the different sialofucosylated and fucosylated O- and N-glycans that were abundantly present in mucus produced on-chip under both flow conditions. (**Fig. 2a**). Importantly, the wide range of mucus O- and N-glycans accumulated on-chip also more closely resembled the heterogeneity of the glycan profiles observed in clinical cervical mucus samples presented here for the mucus obtained from an African American donor (which contain mucus from both ecto- and endo-cervix *in vivo*) compared to the glycan pattern exhibited by samples collected from Transwell cultures. The Transwell mucus also had high abundance of multiple undecorated O-glycans that were not detected in the chip and clinical mucus samples (**Fig. 2a**). Mucus from Cervix Chips contained the most commonly found O- and N-glycans present in the clinical human mucus, including more than 45% (5 of 11) of the O-glycan and 75% (9 of 12) of the N-glycan structures (**Fig. 2b**). These O- and N-glycans exhibited the same structure and configuration (nature, order, and location) of monosaccharide residues, as well as the same compound retention time, in all sample types. Although most of these common structures were also present in Transwell mucus, the sialofucosylated (2_2_1_2|24.7) O-glycan commonly found in clinical mucus was not detected in mucus from Transwell cultures.

Mucus biophysical properties also play an important role in cervical physiology and pathophysiology as the selective permeability of the mucus modulates interactions between the epithelium and overlying bacteria, bacterial products, and viruses in the lower female reproductive tract [17,48,49]. We characterized the viscosity of the Cervix Chip mucus using a single particle tracking (SPT) technique [49] in which fluorescently-labeled carboxylated microparticles (1 µm diameter) were flowed through the epithelial channel and allowed to diffuse into the live mucus on-chip. Phase contrast and fluorescent microscopic imaging of the Cervix Chip revealed that the microparticles distributed themselves throughout the mucus, both axially along the flow direction and vertically throughout the thickness of the mucus layer (**Supplementary Fig. S1h**). Analysis of Brownian movements of the microparticles revealed that the diffusion constant of the mucus produced on-chip when cultured in the presence of high (5 nM) estrogen using the periodic flow regimen was ~ 1 $\times 10^{-13}$ m^2/s, which is comparable to the diffusivity measured in human cervical mucus obtained during ovulatory phase (5.5×10^{-14} m^2/s), whereas the value for mucus produced in static Transwell cultures was significantly higher (~1.6×10^{-13} m^2/s)(**Fig. 2c**). Lower diffusivity is consistent with the chip producing a thicker and more viscous mucus layer. The diffusion exponent of the microparticle[48] was found to be 0.2-0.5 for the Cervix Chip mucus, which indicates a subdiffusive behavior (a measure of macromolecular crowding) that is also comparable to that observed *in vivo* [48]. Thus, the Cervix Chip accumulates a chemically, physically, and physiologically relevant mucus layer *in vitro*.

Modulation of cervical mucus by pH and sex hormone levels

The microenvironment of the lining of the human cervix has a slightly acidic to neutral pH (~ 5.6-7) and elevated pH levels are associated with dysbiotic vaginal microflora that can ascend to the cervix and upper female reproductive tract [50]. When we analyzed mucus from Cervix Chips cultured under continuous flow that exhibit features of ectocervix which is anatomically closer to the vagina and experiences a more acidic pH (~ 3.8-4.5) *in vivo*, we found that the mucus layer more than doubled in

projected area when the cells were cultured at pH 5.4 compared to neutral conditions (pH 7.1) using dark field and fluorescence microscopic side view imaging of WGA-stained cultures (**Fig. 3a**). Measuring the pH at the inlet and outlet of the apical channel of the chip using a digital microprobe pH meter revealed a significant increase in pH from 5.4 in the chip inflow to 6.2 in the outflow (**Supplementary Fig. S2a**), which is comparable to clinically reported pH levels in the human cervix *in vivo* [50]. The acidic pH on-chip did not affect the integrity of the epithelial barrier function or the total amount of Alcian Blue-staining mucus material compared to neutral pH (**Supplementary Fig. S2b,c**). However, real time qPCR analysis revealed a significant (>5-fold) increase in expression of mucin MUC4 and SLPI (>2-fold) in the cervical epithelium differentiated under the acidic pH conditions (**Fig. 3b**), while other major cervical epithelial genes (e.g., MUC5B, ASRGL1(asparaginase and isoaspartyl peptidase 1) remained unchanged (**Supplementary Fig. S2d**). Acidic pH also significantly reduced production of inflammatory TNF-α protein by the cervical epithelium on-chip (**Fig. 3c**) which is similar to the anti-inflammatory effect that acidic pH has been reported to induce in airway epithelial cells [51].

Hormonal fluctuations during the menstrual cycle modulate the cervical microenvironment, including the properties and functions of the cervical mucus [24,25]. Ovulatory and non-ovulatory hormonal phases of the menstrual cycle were simulated in the Cervix Chip exposed to periodic flow (to induce a more endocervical phenotype) by perfusing differentiation medium through the basal channel containing either high (5 nM) β-estradiol (E2) and no progesterone (P4) to mimic the ovulatory phase or low (0.5 nM) E2 and high (50 nM) P4 hormone levels to recreate the non-ovulatory environment [52]. Side view microscopic imaging of the WGA-stained mucus layer showed increased accumulation of mucus on-chip cultured under ovulatory conditions with high E2 compared to low E2/high P4 non-ovulatory conditions (**Fig. 3d**). Quantification of these results confirmed that the mucus layer was significantly thicker (0.33 vs 0.22 mm) and exhibited a higher level of WGA fluorescence signal intensity (27.1 vs 22.1 gray value) under ovulatory versus non-ovulatory conditions (**Fig. 3d,e**). The Cervix Chip mucus also

exhibited a significantly higher amount of Alcian Blue staining mucus material when exposed to ovulatory hormone levels (**Supplementary Fig. S2e**) and this was accompanied by a significantly higher ratio of MUC5B: MUC5AC gene expression (**Supplementary Fig. S2f**).

On-chip analysis of mucus biophysical properties on day 12 of culture also demonstrated a significantly higher diffusion constant in ovulatory compared to non-ovulatory mucus (8.4×10^{-14} versus 5.7×10^{-14} m^2/s) (**Fig. 3f**), which mimics the increase in viscosity similarly observed in clinical mucus when the cycle shifts from the ovulatory to the non-ovulatory phase [24]. Interestingly, using the clinical Fern Test in which vaginal secretions are allowed to dry on a slide[53], we found that mucus effluents from the ovulatory and non-ovulatory chips formed fern-like and granular patterns respectively, which are similar to the patterns formed by ovulatory and non-ovulatory cervical mucus in clinical studies [54] (**Fig. 3g**).

In parallel, we carried out glycomic analysis which revealed that the abundances of the sialylated 2_2_0_2|28.2 and disialofucosylated 2_2_1_2|24.7 decreased while the monosialylated 2_2_0_1|19.3 O-glycans increased in mucus produced under non-ovulatory conditions compared to ovulatory conditions on-chip (**Supplementary Fig. S2g**) suggesting a decrease in sialylation. There also was an overall drop in most of the identified sialylated, sialofucosylated and fucosylated N-glycans in response to exposure to high progesterone levels on-chip. Importantly, these changes in the mucin glycosylation profile are consistent with reported hormone-dependent mucin glycosylation patterns previously observed in clinical samples [25,47].

The ovulatory hormone condition with high E2 was also accompanied by significant upregulation of pro-inflammatory cytokines, including IL-1β, IL-8, and TNF-α proteins on-chip compared to the non-ovulatory condition (**Fig. 3h**), which is consistent with the known ability of estrogens to exhibit pro-inflammatory activities [55]. In addition, the integrity of the cervical epithelial barrier was consistently lower when the chip was cultured under these ovulatory conditions (**Fig. 3i)**, which again is consistent

with the relaxation of the epithelial tight junctions and associated increased fluid flux across the epithelium leading to higher mucus hydration (increased diffusion) that has been reported during ovulatory phase of the cycle [56]. Moreover, when the hormone levels were switched from high estrogen to high progesterone on day 6 of differentiation, the TEER values measured over time in the same cultures using integrated electrodes significantly increased confirming the hormone responsiveness of the cervical epithelial barrier on-chip (**Fig. 3j**).

Colonization of the Cervix Chip by optimal and non-optimal commensal bacterial communities

L. crispatus dominant microbiota are known to be associated with optimal, healthy human cervico-vagina mucosa *in vivo* [35,57], while *G. vaginalis* is commonly found in dysbiotic bacterial communities associated with BV [58]. To model the healthy cervix, we therefore cultured a bacterial consortium containing three optimal *L. crispatus* strains (C0059E1, C0124A1, C0175A1)[59] in chips cultured under periodic flow to mimic the effect of vaginal microbiome on the endocervix which would have the highest relevance for the health of the upper reproductive tract. Dysbiotic conditions were simulated in these chips by culturing a consortium of two non-optimal *G. vaginalis* strains under ovulatory conditions (5 nM E2). Phase contrast and immunofluorescence microscopic imaging of differentiated Cervix Chips colonized with *L. crispatus* for 3 days confirmed that the epithelial cell layer remained intact and cells appeared refractile even though we could detect the presence of bacteria closely associated with MUC5B-containing mucus on the surface of the epithelium (**Fig. 4a**). In contrast, when the *G. vaginalis* consortium was cultured on-chip under similar conditions, we observed a greater abundance of *G. vaginalis* bacteria and this was accompanied by disruption of the epithelial cell layer, cell detachment, and appearance of smaller pyknotic nuclei (**Fig. 4b)**.

The Cervix Chip maintained a stable engrafted population of both *L. crispatus* and *G. vaginalis* bacteria throughout the 3 days of co-culture as determined by quantifying the total number of live culturable bacteria collected every 24 hrs from the apical channel effluents and from epithelial tissue

digests at the end of the experiment compared to the initial inoculum (**Fig. 4c**). This method also confirmed that co-culture of *L. crispatus* bacteria with the epithelium did not affect epithelial cell number whereas colonization with *G. vaginalis* produced a significant loss of cervical epithelial cells compared to control non-inoculated and *L. crispatus* colonized chips (**Fig. 4d**). In contrast, measurement of pH levels in the epithelial channel after 72 hours of co-culture with both *L. crispatus* and *G. vaginalis* showed comparable levels to those in control chips with no bacteria (**Supplementary Fig. S3a**). However, while *L. crispatus* colonization did not affect the epithelial barrier integrity, *G. vaginalis* infection significantly compromised the epithelial barrier at 72 hrs as indicated by an increase in P_{app} when compared to the chips colonized with *L. crispatus* consortia or control chips without bacteria (**Fig. 4e**). In addition, the presence of *G. vaginalis* consortia significantly upregulated production of multiple pro-inflammatory cytokines, including IL-1α, IL-1β, IL-6, IL-8, and TNF-α in the upper channel effluents of the chip, while *L. crispatus* consortia downregulated this inflammatory response compared to the non-inoculated control chip when measured after 3 days of co-culture (**Fig. 4f**).

Modulation of the Cervix Chip mucus by the microbiome

Colonization of the Cervix Chip with *L. crispatus* bacteria resulted in a significant increase in mucus layer thickness and WGA-stained fluorescent signal intensity along the entire length of the chip compared to chips co-cultured with *G. vaginalis* or without any bacteria as visualized on day 3 of co-culture (**Fig. 5a-c**), although there was no significant change in the total mucin content of the effluents from the epithelial channel (**Supplementary Fig. S3b**). Interestingly, Fern Testing of the mucus collected from the chip effluents revealed that colonization with *L. crispatus* increased the length and branching degrees of the mucus ferns (up to quaternary) with more observed crystallization compared to mucus from chips without bacteria, while *G. vaginalis* reduced these features in a manner similar to that previously observed in clinical samples of atypical mucus [60] (**Fig. 5d**). The presence of *L. crispatus* also significantly lowered the mucus diffusion constant and exponent (and hence, increased mucus viscosity

and decreased molecular crowding, respectively) compared to chips with *G. vaginalis* or control chips with no bacteria (**Fig. 5e,f**). The presence of *G. vaginalis* bacteria also significantly reduced the relative abundance of major sialylated O-glycans (e.g., 2_2_0_2|28.9 structure) and this was accompanied by a significant increase in the abundance of multiple undecorated O-glycans (**Fig. 5g,h**). Importantly, similar changes in sialylated O-glycans have been previously observed in BV-associated mucus *in vivo* [25,61]. The loss of sialic acids in the mucus may reduce interactions between mucin molecules and contribute to the changes in the physical properties of mucus (e.g., lower viscosity, decreased fern branching) that we observed in the Cervix Chip.

DISCUSSION

For decades, development of new treatments for dysbiosis, BV, and other reproductive health conditions has been limited by our poor understanding of the complex host-microbiome interactions and the role of cervical mucus in host immunity of the lower reproductive tract. It also has been impossible to tease out contributions from mucus produced by the endo-cervix versus ecto-cervix. Advancements have been held back by the lack of *in vitro* models that faithfully recapitulate the physiology and pathophysiology of the human cervix microenvironments [2,3,10,35]. Here we described development of preclinical human Cervix Chip models that recapitulate the physiology of the endo- and ecto-cervical mucosa as well as their responses to microenvironmental, hormonal, and microbiome influences. The dual-channel design of the microfluidic chip enabled formation of a human cervical mucosa *in vitro* containing stromal cells interfaced with cervical epithelium, which is critical given the known importance of the stroma for control of cervical epithelial growth, function, and hormone-stimulated secretion [10,62]. Indeed, under these conditions we observed formation of a mucus-producing cervical epithelium with a tight permeability barrier that recapitulated many features of the cervical mucosa observed *in vivo*.

Host-induced biomolecular signals (e.g., Wnt) has been previously shown to induce differentiation of distinct endo- and ecto-cervical epithelial lineages [63]. However, by exploring the use of continuous versus episodic flow regimens similar to those that can be experienced in the cervix *in vivo*, we discovered that these dynamic flow conditions provide biomechanical cues that also can significantly influence cervical epithelial cell differentiation as well as mucus composition and innate immune responses. Specifically, we found that periodic flow promoted endo-cervical differentiation on chip while continuous flow induced expression of more ecto-cervical phenotype. These findings are consistent with the profound effects that dynamic fluid flow and other biomechanical cues have been shown to have on differentiation of other types of epithelial cells (e.g., intestine, kidney, etc.)[31,64,65]; however, to our knowledge this has not be studied to date in the context of cervical development. Interestingly, we also found that while periodic flow conditions that included intermittent static periods produced effects that promoted endo-cervical specialization which were more similar to those observed when the same epithelial and stromal cells were cultured in the same medium in static Transwell inserts, there were also distinct differences, including differences in epithelial barrier integrity and mucus composition, with the chip more closely resembling features observed *in vivo*.

Mucus secretion is the primary function of the cervix in the female reproductive tract that protects the epithelium against pathogen invasion. We showed here that the engineered Cervix Chip accumulate thick mucus layers that are amenable to real-time quantitative analysis in terms of their thickness and chemical composition as well as their biophysical properties. This approach revealed that the Cervix Chips respond physiologically to both hormonal and bacterial influences in a manner similar to that observed *in vivo*. The abundance of the mucus produced on-chip allowed for non-invasive longitudinal analysis of its formation as well as collection of both soluble mucus materials that flow out in the effluent of the epithelial channel and adherent mucus that remains adherent to the epithelium when the cultures are sacrificed at the end of the study. This is a major advantage compared to existing

in vitro and *in vivo* models used to study cervix physiology and pathophysiology. By using image-based, biochemical, biophysical, biomolecular, transcriptomic, and glycomic analyses, we were able to demonstrate that the mucus produced in the Cervix Chips faithfully recapitulated multiple features of human cervical mucus produced *in vivo*. In particular, for the first time, high resolution glycomic analysis was used to quantify and characterize cervical mucus glycan subtypes and molecular structures, which also confirmed that the mucus produced on-chip under dynamic flow conditions more closely resembled clinical mucus isolated from cervical samples than that produced by the same cervical cells in static 2D cultures or Transwell. These findings provide a baseline for future studies analyzing how that hormonal, bacterial, or host-derived modulations of mucus glycosylation structure can influence cervico-vaginal physiology and pathophysiology, while much has been previously reported in studies on intestinal mucus-microbiome interactions [66-68]. Importantly, one major advantage of the Organ Chip model is that it allows many potential contributing factors to be varied independently or in combination, which is impossible in animal models or in clinical studies where the effects of mucus cannot be separated from those induced by external bacterial or microenvironmental, nor can contributions of endo-cervical mucus be separated from those produced by ecto-cervical secretions.

Microenvironmental factors, such as pH and hormone fluctuations during menstrual cycle, pregnancy, and menopause, also can modulate intracellular functions of the mammalian cells, mucus properties, and microbial communities, as well as host-microbiome homeostasis [15,69]. Teasing out the contribution of each of these factors in the cervico-vagina-microbiome homeostasis has been almost impossible due to their simultaneous occurrence *in vivo*. Using Cervix Chips, we demonstrated that each of these contributing factors can be independently and physiologically modelled and studied *in vitro*. Importantly, using this more well defined characterization platform, we showed that physiological responses obtained on-chip are similar to those observed *in vivo* [34,70].

With the increasing recognition of the importance of the microbiome for health and disease of the female reproductive and genital tracts [57,71], it is critical to develop *in vitro* models that can be used to study the complex host-microbiome interactions. We leveraged the Cervix Chips to model healthy- and dysbiotic-associated cervical microenvironments *in vitro* using clinically derived isolates of *L. crispatus* (optimal) and *G. vaginalis* (non-optimal) bacterial communities. Colonization of the Cervix Chips resulted in producing of the cervical mucus discharge that closely resembled samples obtained clinically, including similar results in Fern Tests that are commonly used in clinic as diagnostic. While the Cervix Chips co-cultured with optimal *L. crispatus* bacteria exhibited a stable epithelial layer, good barrier function, and a quiescent immune state, as well as production of mucus with clinically relevant composition and biophysical properties, co-culture of chips with disease-associated *G. vaginalis* bacteria resulted in a damaged cervical epithelium, cell death, compromised barrier and altered mucus properties in addition to an enhanced inflammatory response, which are all major phenotypic signatures of a dysbiotic cervix *in vivo* [11,57,72].

Characterization of biophysical properties of the mucus revealed that *L. crispatus* strains decrease two major diffusion behaviors of the mucus on-chip (diffusion constant and exponent), which reflect formation of a more restrictive mucus environment that reduces movement and increases adhesion of the entrapped bacterial and viral substances. Confined diffusion movement and subdiffusive behavior of the mucus has been proposed as one of the fundamental mechanisms of mucosal immunity by creating a physical barrier that traps the bacteria and viruses [73] and facilitates antipathogenic processes conducted through mucus adhesion [48,74]. Destruction of this biophysical barrier mechanism and increased motility of virulence particles in the mucus has been previously shown to be associated with higher risk of acquiring HIV-1 in women with BV [16].

On a biochemical level, we found that *G. vaginalis* significantly reduces the abundance of sialylated O-glycans in the Cervix Chip mucus. Dysbiotic bacteria including *G. vaginalis, Prevotella, and*

Bacteroides express sialidases enzymes [75] that cleave the sialic acid shielding cap of the mucin glycans and making the mucin polymers more vulnerable to further degradation by other dysbiotic bacteria proteases and mucinases enzymes. [25,76,77] This can result in profound effects on the mucus layer, including reduced molecular interactions between the mucin glycoproteins, decreased viscosity, and easier shedding of the mucosal layer from the epithelial surface. The effect of *L. crispatus* on the cervical mucus and its glycosylation profile is, however, not fully understood, aside from its known positive effect in protection against pathogens[78]. We showed that colonization of the Cervix Chip with *L. crispatus* maintains a high level of sialylated O-glycans, essential for mucosal protection against dysbiotic bacteria and pathogens aggression[79]. In addition, this study revealed that these optimal *L. crispatus* communities may protect against pathogenic bacteria by inducing formation of a thicker, less diffusive mucosal layer and by enhancing innate immunity.

Taken together, the Cervix Chip models provide experimental platforms for study of human cervical physiology and pathophysiology that far surpass the previously reported *in vitro* models in terms of their ability to recapitulate endo- and ecto-cervical epithelial differentiation, barrier formation, mucus production, and functional responses to hormonal, microenvironmental and bacterial stimuli. While *in vitro* models of the cervix have been used previously to study host responses to healthy- and diseased-associated bacteria and microbicides [30,80] they lacked an *in vivo* like cervical epithelial-stromal interface and failed to demonstrate clinically relevant mucus production. Taken together, these findings suggest that these microfluidic human Cervix Chips that offer many advantages over conventional culture systems may provide ideal preclinical models for analysis of host-microbiome interactions as well as test beds for biotherapeutic treatments and interventions that aim to treat BV and improve reproductive health among millions of women around the world.

METHODS

Cervix Chip seeding and culture. A microfluidic organ chip (Emulate, CHIP-S1™) made of transparent, flexible polydimethylsiloxane (PDMS), and constitute of two parallel microchannels (1 mm wide × 1 mm high apical channel and a 1 mm wide × 0.2 mm high basal channel) separated by a porous membrane (50 µm thickness, 7 µm pores with 40 µm spacing) similar to a previously published design[81] was used to create the Cervix Chip model. Before cell seeding, the polymeric surfaces of the membrane were chemically functionalized with 0.5 mg/ml ER1 in ER2 buffer (Emulate™ Inc., USA) polymerized under an ultraviolet lamp (Nailstar, NS-01-US) for 15 min following by sequential washing with ER2 buffer and PBS. The PDMS membrane was coated with 500 µg/ml collagen IV (Sigma-Aldrich, Cat. no. C7521) in the apical channel and with 200 µg/ml Collagen I (Advanced BioMatrix, Cat. no. 5005) and 30 µg/ml fibronectin (Corning, Cat. no. 356008) in DPBS in the basal channel overnight at 37°C. The channels were washed with DPBS and culture medium before seeding cells.

Primary cervical epithelial (CE) cells (LifeLine Cell Technology Cat# FC-0080, Donors ID: 6225, 6226, 6227) that contain a mixture of ecto- and endo-cervical epithelial cells were expanded in cervical expansion medium composed of a cervical basal medium (LifeLine Cell Technology, LM-0055) supplemented with cervical growth factors (LifeLine Cell Technology, SKU:LL-0072) and 50 U/ml Penicillin-Streptomycin (Gibco™, 15070063). Primary cervical fibroblast (CF) cells, isolated from healthy cervical tissue-obtained from hysterectomy procedure, using a previously described method[82], were expanded in fibroblast expansion medium; fibroblast basal medium (ATCC® PCS-201-030™) supplemented with fibroblast growth factors (ATCC® PCS-201-041™) and 50 U/ml Penicillin-Streptomycin (Gibco™, 15070063).

To create the Cervix Chips, primary cervical fibroblasts (P5, 0.65 x10^6 cells/ml) were first seeded on the basal side of the porous membrane by inverting the chip for 2 hours in fibroblast cell growth medium to allow attachment of the cells to the porous membrane, followed by flipping the chips again

and seeding the primary cervical epithelial cells (P5, 1.5 x 10^6 cells/ml) on the apical side for 3 hours in epithelial cell growth medium. The respective media of the chips were refreshed for each channel and the chips were incubated at 37°C, 5% CO_2 under static conditions overnight. The chips were then connected to the culture module instrument (ZOË™ CULTURE MODULE, Emulate Inc.,USA) to enable controlled perfusion of medium in the chips using pressure driven flow. The Cervix Chips were cultured using a periodic flow regimen in which cervical growth medium was flowed through the apical channel for 4 hours per day at 30 µl/hr with continuous flow of fibroblast growth medium basally at 40 µl/hr or using a continuous flow regimen that involved continuous perfusion of both apical and basal channels with the same respective media but at 40 µl/hr. After 5 days the apical medium was replaced by Hank's Buffer Saline Solution (HBSS) (Thermo Fisher, 14025076) while being fed through the basal channel by constant flow of cervical epithelial medium (LifeLine Cell Technology, Cat. no. LL-0072) supplemented with 5 nM female sex hormone estradiol-17β (E2) (Sigma, Cat. no. E2257) to promote epithelial differentiation and 50 µg/mL Ascorbic acid (ATCC, Cat. no. PCS-201-040) to support stromal fibroblast growth and increase collagen synthesis in continuous regimen cultures [83]. Under both flow regimens, the apical medium was replaced at day 2 of differentiation by a customized HBSS with low buffering salts and no glucose (HBSS (LB/-G) with pH ~5.4 to better mimic the acidic microenvironment of the cervix *in vivo* and then the chips were cultured for 5 additional days (7 total days under differentiation conditions; 12 days of culture on-chip). The chip cultures were maintained in an incubator containing 5% CO_2 and 16–18% O_2 at 85–95% humidity. The pH of the chip inflows and effluents for apical and basal channels were measured using SevenGoDuo SG68-B pH meter with InLab Ultra-Micro-ISM probe (METTLER TOLEDO, USA).

Immunofluorescence microscopy. Cervix Chips or cells were first washed with DPBS in the apical and basal channels, fixed with 4% paraformaldehyde (FisherScientific, Cat. no. 50-980-487) for 20 min before being washed with DPBS and storage at 4°C. The chips and cells were permeabilized with

0.05% triton X-100 (Sigma) in Tris-buffered saline (TBS) for 10 min at room temperature, then blocked in 5% normal donkey serum (Sigma-Aldrich, D9663), for one hour at room temperature, followed by overnight incubation in primary-antibodies diluted in 5% donkey serum at 4^{o}C on a rocking plate. The samples were then incubated with corresponding secondary-antibody for 1 hour at room temperature; the nuclei were stained with Hoescht 33342 (Life Technologies, H3570, 1:1000) in diH2O for 10 min at room temperature after secondary-antibody staining. Fluorescence imaging was performed using a confocal laser-scanning microscope (Leica SP5 X MP DMI-6000) following by image processing using the Imaris software (Bitplane). Primary antibodies used in these studies included ones directed against MUC5B (Abcam, Cat. no. ab87376), KI67 (Thermo Scientific, Cat. no. RM-9106-S), cytokeratin 18 (Abcam, Cat. no. ab668), cytokeratin 7 (Cat. No. ab209601), cytokeratin 14 (Cat. No. ab51054), F-actin (Abcam, Cat. no. ab176757), vimentin (Abcam, Cat. no. 195878), estrogen receptor (Abcam, Cat. no. ab32063), and progesterone receptor (Abcam, Cat. no. ab2765). Secondary antibodies included Donkey anti-rabbit Alexa Flour 647 (Jackson lab, Cat. no. 715-605-151 and 715-605-152) and Donkey anti-rabbit Alexa Flour 488 (ThermoFisher, Cat. no. A21206).

Epithelial barrier function. Real-time trans-epithelial electrical resistance (TEER) was measured in Cervix Chips using an in-house TEER-sensor integrated Organ Chip device developed based on our previous TEER-integrated OOC system[42]. Briefly, the TEER-integrated sensor chips constitute of dual microfluidic channels with the design dimensions described earlier. Gold electrodes patterned on polycarbonate substrate were integrated into the chips following a layer-by-layer assembly approach that places three electrodes on each side of the cervical epithelium-stroma layer. The TEER-sensor chip was mounted on a printed circuit board (PCB) and assembled into a standalone Organ Chip unit that was multiplexed and directly connected to an external potentiostat, which enabled real-time and remote TEER measurements of the Cervix Chips from outside the incubator throughout the culture time. TEER measurements were performed by applying an electrical current (10 μA) to the chip and through one set

of electrodes at a frequency sweep of 10 to 10000 Hz and measuring the drop in the potential by another set of electrodes in the chip using a PGStat 12/FRA (Autolab). Four-point impedance measurements were taken periodically throughout the culture time using IviumSoft (Ivium Technologies). The cervical epithelium TEER was presented as corrected TEER obtained from measured impedance at 100 Hz subtracted from that measured at 100000 Hz, which represent the chip media resistance. At <100 Hz frequency the impedance signal is dominated by the TEER [42]. TEER of the cervical epithelial cells on Transwell was measured using the EVOM^2 Epithelial Voltohmmeter and EndOhm Culture Cup Chamber (WPI, USA).

To measure epithelium paracellular permeability (P_{app}), Cascade Blue tracer dye (Cascade Blue® hydrazide, trilithium salt; ThermoFisher, C3239) was introduced to the apical medium at 50 µg/ml and perfused through the epithelial channel of the chip. 40 µl of the apical and basal channels of the chip effluents were collected and their fluorescent intensities (390nm/420nm) were measured with a multimode plate reader (BioTek NEO) at each timepoint throughout the culture. P_{app} was calculated based on a standard curve and the following equation, as previously described [84]:

$$P_{app} = \frac{V_r \times C_r}{A \times t \times \frac{(C_{d-out} \times V_d + C_r \times V_r)}{(V_d + V_r)}}$$

Where, V_r (mL) is volume of receiving channel at time t (s), V_d (mL) is volume of dosing channel at time t, A (cm^2) is the area of membrane (0.167 cm^2), C_r (µg/mL) is the measured concentration of the tracer in the receiving channel, and $C_{d\text{-}out}$ (µg/mL) is measured concentration of tracer in the dosing channel effluent.

Live mucus imaging on-chip. To visualize live cervical mucus in the Cervix Chip, fluorescent wheat germ agglutinin (WGA) (25 µg/ml, Invitrogen, Cat. no. W11261) was perfused through the apical epithelium channel at 30µl/hr flow rate for 1 hour followed by HBSS wash for 30 min-1 hr. The chips were then cut on the sides parallel to the length of the main channel and rotated on one side on a cover

glass coated with PBS, additional PBS was applied to the top side of the chip and covered with a cover glass as described previously in [31]. Dark field and fluorescence images were acquired with an inverted microscope (Axial observer Z1 Zeiss) with LD PlnN 5X/0.4 Ph2 objective lens, and OCRA-Flash4.0 C11440 Hamamatsu digital camera. Quantitative mucus area analysis was performed using Fiji software.

Mucus collection. Cervical mucus was collected using 20mM N-acetylcysteine (NAC) (Sigma, A9165) in DPBS that was perfused though the apical epithelial channel of the chip or added to the Transwell apical chamber and incubated for 3 hours before collection. Collected mucus samples were used in total mucin quantification using Alcina blue assay and glycomic profile analysis using Agilent nanoscale liquid chromatography quadrupole time-of-flight coupled to tandem mass spectrometry (nanoLC-QTOF MS/MS).

Alcian Blue mucin assay. The total mucin content was determined following the method described in [41] by equilibrating the collected chip mucus samples with Alcian Blue stain (ThermoFisher, 88043) for 2 hours, followed by centrifuging the resulting precipitant at 1870g for 30 min, then 2X wash/spin cycles with a washing solution composed of 40% ethanol, 0.1 mol/L acetic acid, and 25 mmol/L magnesium chloride. The stained mucin pellets were then dissociated in 10% sodium dodecyl sulfate solution (Sigma, 71736), and the absorbance was measured with a microplate reader (Syn-Q55 ergy HT, BioTek) at 620 nm. Mucin concentrations were obtained based on a curve fitted to mucin standards developed from submaxillary gland mucin (sigma) serially diluted from 0 to 500 µg/ml, and Alcian Blue stained as described above.

Mucus Fern Test. Mucus ferning pattern was qualitatively analyzed by using 10µl of undiluted apical effluent that was deposited on a micro cover glass (BRAND®, cat no 4708 20). The drop was manually spread using a pipette tip and allowed to dry in room air for 1 hour before the ferning patterns were visualized on Revolve microscope (Revolve Software V6.0.1) in the inverted mode.

Gene expression analysis. Total RNA was isolated from the cell lysate of the cervical epithelial cells of chips and Transwells at day 7 of differentiation, using RNeasy Micro Kit (QIAEGN, Cat. No. 74004), followed by complimentary DNA synthesis using SuperScript VILO MasterMix (Invitrogen, cat. No. 11755-050). Cellular gene-expression levels were determined using RT-qPCR according to the TaqMan fast Advanced Master mix (Thermofisher, Cat. No. 4444963) with 20 µl of reaction mixture containing gene-specific primers for mucin 5B (MUC5B, Hs00861595), mucin 4 (MUC4, Hs00366414), L-asparaginase enzyme (ASRGL1, Hs01091302), and secretory leukocyte peptidase inhibitor (SLPI, Hs01091302). The expression levels of the target gene were normalized to GAPDH.

To analyze differential gene expression, total RNA samples (150-300 ng/sample) from Cervix Chips and Transwells were submitted to Genewiz commercial sequencing facility (South Plainfield, NJ) for Next Generation Sequencing (NGS). All submitted samples had an RNA integrity number (RIN) > 8.9. Stranded TruSeq cDNA libraries with poly dT enrichment were prepared from total RNA from each sample according to the manufacture's protocol. Libraries for the 37 cDNA samples were sequenced using the Illumina HiSeq sequencing platform yielding 20-30 million 150 bp paired end (PE) sequence reads per sample. Reads have been mapped to Ensembl release 86 using STAR (v2.5.2b) read counts have been generated using the featureCounts of Subread package (v2.0.3) and analyzed using a custom bioinformatics workflows implemented in R (v3.6.3). Read counts have been normalized across libraries using the median ratios method implemented in DESeq2 (v.1.26.0), and ggplot2 (v3.3.5) and pheatmap (v1.0.12) packages have been used to create figures and heatmaps.

Analysis of cytokines and chemokines. The epithelial effluents from the Cervix Chip were collected and analyzed for a panel of cytokines and chemokine-INF-γ, IL-1α, IL-1β, IL-10, IL-6, IL-8, and TNF-α – using a custom U-PLEX® Biomarker Assay kit (Mesoscale Discovery, cat. No. K15067L-1). The analyte concentrations were determined using a MSD Model 1300 instrument coupled with Discovery Workbench 4.0.12 software.

Glycomic analysis. *N-glycan release.* The samples were transferred to pre-rinsed Amicon Ultra-0.5 (10kDa) centrifugal filter units (MilliporeSigma, MA) and cleaned up with 400 µL of nanopure water followed by centrifugation at 14,000 × g for 15 min three times to remove salts. The protein samples were then recovered by reverse-spinning the unit at 1,000 × g for 2 min. As described previously[85], dithiothreitol (DTT) and NH_4HCO_3 were added to the purified samples to final concentrations of 5 mM and 100 mM, respectively. The mixture was heated in a boiling water bath for 2 min to denature the proteins. For N-glycan release, 2 µL of PNGase F (New England Biolabs, MA) was added, and the samples were incubated at 37°C in a microwave reactor (CEM Corporation, NC) for 10 min at 20 W. The samples were further incubated in a 37 °C water bath overnight to fully convert the glycan's amine group to hydroxyl group. After the incubation, 350 µL of nanopure water was added and ultracentrifuged at 200,000 × g for 45 min at 4°C. The protein pellets were saved for O-glycan release. The supernatant containing the released N-glycans was desalted with porous graphitized carbon (PGC) solid-phase extraction (SPE) plates (Glygen, MD). The PGC-SPE plate was activated by 80% (v/v) acetonitrile (ACN) and equilibrated with water prior to use. The N-glycans were washed with 3 vol. of water, eluted with 40% (v/v) ACN, and dried in vacuo. *O-glycan release.* The de-N-glycosylated protein pellets were resuspended in 90 µL of nanopure water by sonication for 20 min. 10 µL of 2 M NaOH and 100 µL of 2 M $NaBH_4$ were added and the mixture was incubated in a 45°C water bath for 18 h. The reaction was quenched by mixing with 100–120 µL of 10% acetic acid on ice until the pH values reached 4–6. Then the samples were centrifuged at 21,000 × g for 30 min at 4°C. The supernatant containing the released O-glycans was desalted with PGC-SPE plates (Glygen, MD), and further purified with iSPE-HILIC cartridges (Nest Group, MA). The HILIC cartridges were activated with ACN and water and equilibrated with 90% (v/v) ACN. The dried O-glycan eluates from PGC SPE were reconstituted in 90% (v/v) ACN and allowed to pass through the HILIC cartridges five times. The O-glycans were then washed with 5 vol. of 90% (v/v) ACN, eluted with water, and dried in vacuo.

Glycomic analysis with LC-MS/MS was employed as previously described[46]. In general, the glycan samples were reconstituted in 8 µL of nanopure water and analyzed with an Agilent 1200 series HPLC-Chip (PGC) system coupled to an Agilent 6520 Accurate-Mass Q-TOF MS (Agilent, CA). The glycans were first loaded onto the chip with aqueous mobile phase A, 3% (v/v) ACN and 0.1% (v/v) formic acid (FA) in water, at a flow rate of 3 µL/min, and then separated using a binary gradient with the same mobile phase A and organic mobile phase B, 90% (v/v) ACN and 1% (v/v) FA in water, at a flow rate of 0.3 µL/min. The binary gradient was 0.0–2.5 min, 1% (B); 2.5–20.0 min, 1–16% (B); 20.0–35.0 min, 16–58% (B); 35.0–40.0 min, 58–100% (B); 40.0–50.0 min, 100–100% (B); 50.0–50.1 min, 100–1% (B); 50.1–65.0 min, 1–1% (B). The drying gas temperature and flow rate were set at 325°C and 5 L/min, respectively. The capillary voltage was adjusted between 1850–2000 V to maintain a stable electrospray. MS spectra were acquired over a mass range of *m/z* 600–2000 for N-glycans and *m/z* 400–2000 for O-glycans in positive ionization mode at a scan rate of 1.25 s/spectrum. Four most abundant precursor ions were fragmented through collision-induced dissociation (CID) with nitrogen gas. MS/MS spectra were collected over a mass range of *m/z* 100–2000 at 1 s/spectrum.

Glycan compound chromatograms were extracted from the raw data using the MassHunter Qualitative Analysis B.08 software (Agilent, CA) with in-house libraries containing common N- and O-glycan accurate masses. N-glycans were identified using the Find by Molecular Feature algorithm with a 20 ppm mass tolerance, and O-glycans the Find by Formula algorithm with a 10 ppm mass tolerance. The glycan structures were confirmed by tandem MS spectra. The relative abundance of each glycan was calculated by normalizing its peak area to the total peak area of all glycans identified.

Single Particle Tracking analysis. *Experimental procedure.* To measure the biophysical properties of the live mucus on-chip, fluorescent, negatively charged (carboxylated) microspheres (Ø= 1µm (Cat. No. CAF-001UM, Magsphere, Inc., Pasadena, CA, USA) was diluted in sterile deionized water at 1:400 (microparticles:dH_2O) followed by 1:30 (microparticle solution: apical medium) dilution in the

apical medium vortexed for 30 sec for adequate mixing. The microparticle containing medium was perfused through the apical epithelial channel of the chip at 30 µl/hr for 2 hours to achieve a uniform distribution of the particles throughout the mucus. Time lapse microscopy imaging was performed at 30.3 frames per second for 10 s for each field of view on chip using an inverted microscope (Axial observer Z1 Zeiss) with LD PlnN 20X/0.4 Ph2 objective lens, and OCRA-Flash4.0 C11440 Hamamatsu digital camera.

At least 10-12 fields of view were imaged on each chip for averaged representative analysis. All image frames were run through a modified version of a publicly available single particle tracking (SPT) Matlab code[86] to identify particles. The code identifies particles using the brightest pixels and filters them using criteria such as feature size and intensity threshold. The x and y positions of every retained particle were refined using the intensity-weighted centroid surrounding the brightest pixels. Particle positions in adjacent frames are linked to form particle trajectories using criteria such as maximum particle displacement and minimum particle trajectory length. A drift correction code from another publicly available source[87] was subsequently applied to all SPT data. This correction subtracts the center of mass motion of all of the particles in a given time frame from each individual trajectory. Using these drift-corrected data, the time averaged mean squared displacement (TAMSD; in two dimensions (2D)) of the jth particle for a movie with M images is given by[88,89].

$$\overline{\Delta r_j^2(\Delta\tau)} = \frac{1}{M - \frac{\Delta\tau}{\Delta t}} \sum_{i=1}^{M-\frac{\Delta\tau}{\Delta t}} \left[(x_j(i\Delta t + \Delta\tau) - x_j(i\Delta t))^2 + (y_j(i\Delta t + \Delta\tau) - y_j(i\Delta t))^2\right], \qquad (1)$$

where Δt is the time between successive frames and $\Delta\tau$ is the lag time. The ensemble-averaged TAMSD (MSD) over all N tracked particles is then

$$< \overline{\Delta r^2(\Delta\tau)} >= \frac{1}{N} \sum_{j=1}^{N} \overline{\Delta r_j^2(\Delta\tau)}. \qquad (2)$$

The MSD is fitted to the general 2D power-law form as

$$< \Delta r^2(\Delta\tau) >= 4D_\alpha \Delta\tau^\alpha, \quad (3)$$

where D_α is a generalized diffusion coefficient[90]. When α<1, the motion of the particle is subdiffusive, and when α>1, the motion is superdiffusive. When α=1, the diffusion is termed normal diffusion or Brownian motion.

Bacterial co-culture on-chip. To mimic and study the co-culture of an optimal vaginal microbiota on the Cervix Chip, a consortium of three *L. crispatus* strains (C0059E1, C0124A1, C0175A1; C6) was constructed that were originally cultivated from women with stable *L. crispatus* dominant microbiota participated in UMB-HMP study [59]. To mimic and study the infection of a non-optimal vaginal microbiota, a *Gardnerella vaginalis* (*G. vaginalis*) consortium was constructed from two *G. vaginalis* strains (*G. vaginalis* E2 and *G. vaginalis* E4), originally isolated from women with diverse, non-L. crispatus consortia participated in UMB-HMP study[59]. Infection inoculum of *L. crispatus* and *G. vaginalis* consortia were made by combining required volumes of each strain to create equal cell density of each *L. crispatus* or *G. vaginalis* strain per 1 ml of inoculum. The bacteria were washed and resuspended in HBSS (LB/+G) to make 2X concentration inoculum on ice. The Cervix Chip mucus was collected from the chips and mixed with the 2X inoculum (1:1) to make the 1X inoculum. Apical epithelium channel of the Cervix Chip was inoculated with *L. crispatus* consortia at 5.9 x 10^6 CFU/ml or with *G. vaginalis* consortia at 1.9 x 10^6 CFU/ml at day 7 of differentiation. The infected chips were maintained under static culture for 20 hours at 37°C and 5% CO_2 following by 72 hours of co-culture under episodic apical flow and continuous basal flow on the Zoe culture module. At 24-, 48-, and 72-hours post inoculation, the Cervix Chip was perfused apically with customized HBSS (LB/+G) for 4 hours at 30 µl/hr to quantify the non-adherent bacterial CFU in the chip effluents at each timepoint. The adherent bacteria were measured at 72 hours post inoculation within the chip epithelial cells digested with Collagenase IV (Gibco, Cat. No. 17104019) in TrypLE (Thermo Fisher, Cat. No. 12605010) at final concentration of 1 mg/ml for 1.5 hours at 37°C and 5% CO_2.

Bacterial strain infection stocks were made following the method described in [33]. Colony forming unites (CFU)/ml of the bacteria collected from the chip effluents and epithelial cell digest was enumerated by spread plating the samples on MRS agar (Hardy, cat. no. G117) for *L. crispatus* samples and on Brucella blood agar (with hemin and vitamin K_1) (Hardy, cat. no. W23) for *G. vaginalis* samples under anaerobic conditions. The colonies were counted after 72 hours of incubation at 37°C and CFU/mL was calculated for each species.

The number of epithelial cells in the Cervix Chip was obtained by digesting the Cervix Chip apical channel at day 7 of differentiation with Collagenase IV (Gibco, Cat. No. 17104019) in TrypLE (Thermo Fisher, Cat. No. 12605010) at a final concentration of 1 mg/ml for 1.5 hours at 37°C and 5% CO_2. The total number of cells was quantified in the collected cell suspension using Trypan Blue staining assay and Hemocytometer.

Statistical analysis. All results are presented from at least two independent experiments and data points are shown as mean ± standard error of the mean (s.e.m.) from multiple biological replicates or Organ Chips. Statistical analysis was performed using GraphPad Prism version 8.0 (GraphPad Software Inc., San Diego, CA) and the statistical significances between groups were tested using two-tailed Student's *t*-test or One-way ANOVA with Bonferroni correction for multiple hypothesis testing, and all *P* values are presented in the figures. Quantitative image analysis was done using Fiji version 1.8.

ACKNOWLEDGMENTS

We thank T. Ferrante for his guidance with microscopy imaging and analysis, David Chou for providing clinical mucus samples, A. Naziripour, B. Lobamba, and R. Prantil-Baun for their help and inputs in the early stages of the project, and Drs. J. Ravel and S. Rakoff-Nahoum Lab for providing the initial strains of *L. crispatus* and *G. vaginalis*. We acknowledge research funding from Bill and Melinda Gates Foundation (to D.E.I.), Canada's Natural Science and Engineering Research Council (NSERC) (to Z.I.), and the Wyss Institute for Biologically Inspired Engineering at Harvard University (to D.E.I.).

COMPETING INTERESTS

D.E.I. holds equity in Emulate, chairs its scientific advisory board and is a member of its board of directors.

REFERENCES

1 Ravel, J. *et al.* Vaginal microbiome of reproductive-age women. *Proc Natl Acad Sci U S A* **108 Suppl 1**, 4680-4687, doi:10.1073/pnas.1002611107 (2011).

2 Bradshaw, C. S. & Sobel, J. D. Current Treatment of Bacterial Vaginosis-Limitations and Need for Innovation. *J Infect Dis* **214 Suppl 1**, S14-20, doi:10.1093/infdis/jiw159 (2016).

3 Peebles, K., Velloza, J., Balkus, J. E., McClelland, R. S. & Barnabas, R. V. High Global Burden and Costs of Bacterial Vaginosis: A Systematic Review and Meta-Analysis. *Sex Transm Dis* **46**, 304-311, doi:10.1097/olq.0000000000000972 (2019).

4 Myer, L., Kuhn, L., Stein, Z. A., Wright, T. C., Jr. & Denny, L. Intravaginal practices, bacterial vaginosis, and women's susceptibility to HIV infection: epidemiological evidence and biological mechanisms. *Lancet Infect Dis* **5**, 786-794, doi:10.1016/s1473-3099(05)70298-x (2005).

5 Cherpes, T. L., Meyn, L. A., Krohn, M. A., Lurie, J. G. & Hillier, S. L. Association between acquisition of herpes simplex virus type 2 in women and bacterial vaginosis. *Clin Infect Dis* **37**, 319-325, doi:10.1086/375819 (2003).

6 Hillier, S. L. *et al.* Association between bacterial vaginosis and preterm delivery of a low-birth-weight infant. The Vaginal Infections and Prematurity Study Group. *N Engl J Med* **333**, 1737-1742, doi:10.1056/nejm199512283332604 (1995).

7 Martin, H. L. *et al.* Vaginal lactobacilli, microbial flora, and risk of human immunodeficiency virus type 1 and sexually transmitted disease acquisition. *J Infect Dis* **180**, 1863-1868, doi:10.1086/315127 (1999).

8 Donders, G. G. *et al.* Predictive value for preterm birth of abnormal vaginal flora, bacterial vaginosis and aerobic vaginitis during the first trimester of pregnancy. *Bjog* **116**, 1315-1324, doi:10.1111/j.1471-0528.2009.02237.x (2009).

9 Fredricks, D. N., Fiedler, T. L. & Marrazzo, J. M. Molecular identification of bacteria associated with bacterial vaginosis. *N Engl J Med* **353**, 1899-1911, doi:10.1056/NEJMoa043802 (2005).

10 Herbst-Kralovetz, M. M., Pyles, R. B., Ratner, A. J., Sycuro, L. K. & Mitchell, C. New Systems for Studying Intercellular Interactions in Bacterial Vaginosis. *Journal of Infectious Diseases* **214**, S6-S13, doi:10.1093/infdis/jiw130 (2016).

11 Anahtar, M. N. *et al.* Cervicovaginal bacteria are a major modulator of host inflammatory responses in the female genital tract. *Immunity* **42**, 965-976, doi:10.1016/j.immuni.2015.04.019 (2015).

12 Larsen, B. & Monif, G. R. G. Understanding the Bacterial Flora of the Female Genital Tract. *Clinical Infectious Diseases* **32**, e69-e77, doi:10.1086/318710 (2001).

13 Ma, B. *et al.* A comprehensive non-redundant gene catalog reveals extensive within-community intraspecies diversity in the human vagina. *Nat Commun* **11**, 940, doi:10.1038/s41467-020-14677-3 (2020).

14 Edwards, V. L. *et al.* The Cervicovaginal Microbiota-Host Interaction Modulates Chlamydia trachomatis Infection. *mBio* **10**, doi:10.1128/mbio.01548-19 (2019).

15 Nakano, F. Y., Leão, R. d. B. F. & Esteves, S. C. Insights into the role of cervical mucus and vaginal pH in unexplained infertility. *MedicalExpress* **2** (2015).

16 Hoang, T. *et al.* The cervicovaginal mucus barrier to HIV-1 is diminished in bacterial vaginosis. *PLoS pathogens* **16**, e1008236 (2020).
17 Lacroix, G., Gouyer, V., Gottrand, F. & Desseyn, J.-L. The Cervicovaginal Mucus Barrier. *International Journal of Molecular Sciences* **21**, 8266 (2020).
18 Radtke, A. L., Quayle, A. J. & Herbst-Kralovetz, M. M. Microbial products alter the expression of membrane-associated mucin and antimicrobial peptides in a three-dimensional human endocervical epithelial cell model. *Biol Reprod* **87**, 132, doi:10.1095/biolreprod.112.103366 (2012).
19 Franklin, R. & Kutteh, W. Characterization of immunoglobulins and cytokines in human cervical mucus: influence of exogenous and endogenous hormones. *Journal of reproductive immunology* **42**, 93-106 (1999).
20 Akiyama, K. *et al.* Molecular detection of microbial colonization in cervical mucus of women with and without endometriosis. *Am J Reprod Immunol* **82**, e13147, doi:10.1111/aji.13147 (2019).
21 Smirnova, M. G., Guo, L., Birchall, J. P. & Pearson, J. P. LPS up-regulates mucin and cytokine mRNA expression and stimulates mucin and cytokine secretion in goblet cells. *Cellular Immunology* **221**, 42-49, doi:https://doi.org/10.1016/S0008-8749(03)00059-5 (2003).
22 Gajer, P. *et al.* Temporal dynamics of the human vaginal microbiota. *Science translational medicine* **4**, 132ra152-132ra152 (2012).
23 Gliniewicz, K. *et al.* Comparison of the vaginal microbiomes of premenopausal and postmenopausal women. *Frontiers in microbiology* **10**, 193 (2019).
24 Chappell, C. A. *et al.* The effects of reproductive hormones on the physical properties of cervicovaginal fluid. *Am J Obstet Gynecol* **211**, 226.e221-227, doi:10.1016/j.ajog.2014.03.041 (2014).
25 Moncla, B. J., Chappell, C. A., Debo, B. M. & Meyn, L. A. The effects of hormones and vaginal microflora on the glycome of the female genital tract: cervical-vaginal fluid. *PLoS One* **11**, e0158687 (2016).
26 Eade, C. R. *et al.* Identification and characterization of bacterial vaginosis-associated pathogens using a comprehensive cervical-vaginal epithelial coculture assay. *PLoS One* **7** (2012).
27 Fichorova, R. N., Yamamoto, H. S., Delaney, M. L., Onderdonk, A. B. & Doncel, G. F. Novel vaginal microflora colonization model providing new insight into microbicide mechanism of action. *MBio* **2**, e00168-00111 (2011).
28 Arslan, S. Y. *et al.* Novel three dimensional human endocervix cultures respond to 28-day hormone treatment. *Endocrinology* **156**, 1602-1609, doi:10.1210/en.2014-1840 (2015).
29 Barrila, J. *et al.* Organotypic 3D cell culture models: using the rotating wall vessel to study host–pathogen interactions. *Nature Reviews Microbiology* **8**, 791-801 (2010).
30 Łaniewski, P. & Herbst-Kralovetz, M. M. Bacterial vaginosis and health-associated bacteria modulate the immunometabolic landscape in 3D model of human cervix. *npj Biofilms and Microbiomes* **7**, 88, doi:10.1038/s41522-021-00259-8 (2021).
31 Sontheimer-Phelps, A. *et al.* Human Colon-on-a-Chip Enables Continuous In Vitro Analysis of Colon Mucus Layer Accumulation and Physiology. *Cellular and Molecular Gastroenterology and Hepatology* **9**, 507-526, doi:10.1016/j.jcmgh.2019.11.008 (2020).
32 Jalili-Firoozinezhad, S. *et al.* A complex human gut microbiome cultured in an anaerobic intestine-on-a-chip. *Nature biomedical engineering* **3**, 520 (2019).
33 Mahajan, G. *et al.* Vaginal microbiome-host interactions modeled in a human vagina-on-a-chip. *Microbiome* **10**, 201, doi:10.1186/s40168-022-01400-1 (2022).
34 Gipson, I. K. Mucins of the human endocervix. *Front Biosci* **6**, D1245-1255, doi:10.2741/gipson (2001).

35 Vagios, S. & Mitchell, C. M. Mutual Preservation: A Review of Interactions Between Cervicovaginal Mucus and Microbiota. *Frontiers in Cellular and Infection Microbiology*, 645 (2021).
36 Murta, E. F., Filho, A. C. & Barcelos, A. C. Relation between vaginal and endocervical pH in pre- and post-menopausal women. *Arch Gynecol Obstet* **272**, 211-213, doi:10.1007/s00404-005-0740-4 (2005).
37 Xiao, S. *et al.* A microfluidic culture model of the human reproductive tract and 28-day menstrual cycle. *Nat Commun* **8**, 14584-14584, doi:10.1038/ncomms14584 (2017).
38 Ostedgaard, L. S. *et al.* Gel-forming mucins form distinct morphologic structures in airways. *Proceedings of the National Academy of Sciences* **114**, 6842-6847 (2017).
39 Gipson, I. K. *et al.* Mucin genes expressed by human female reproductive tract epithelia. *Biol Reprod* **56**, 999-1011, doi:10.1095/biolreprod56.4.999 (1997).
40 Devins K, S. L. H. Cervix General Histology. *PathologyOutlines.com website.* (2020).
41 Hall, R. L. *et al.* A colorimetric assay for mucous glycoproteins using Alcian Blue. *Biochemical Society Transactions* **8**, 72-72, doi:10.1042/bst0080072 (1980).
42 Henry, O. Y. *et al.* Organs-on-chips with integrated electrodes for trans-epithelial electrical resistance (TEER) measurements of human epithelial barrier function. *Lab on a Chip* **17**, 2264-2271 (2017).
43 Ghanem, R. *et al.* Optimizations of In Vitro Mucus and Cell Culture Models to Better Predict In Vivo Gene Transfer in Pathological Lung Respiratory Airways: Cystic Fibrosis as an Example. *Pharmaceutics* **13**, doi:10.3390/pharmaceutics13010047 (2020).
44 Lõhmussaar, K. *et al.* Patient-derived organoids model cervical tissue dynamics and viral oncogenesis in cervical cancer. *Cell Stem Cell* **28**, 1380-1396.e1386, doi:10.1016/j.stem.2021.03.012 (2021).
45 Foroutan, M. *et al.* Single sample scoring of molecular phenotypes. *BMC Bioinformatics* **19**, 404, doi:10.1186/s12859-018-2435-4 (2018).
46 Li, Q., Xie, Y., Wong, M., Barboza, M. & Lebrilla, C. B. Comprehensive structural glycomic characterization of the glycocalyxes of cells and tissues. *Nature Protocols* **15**, 2668-2704, doi:10.1038/s41596-020-0350-4 (2020).
47 Andersch-Björkman, Y., Thomsson, K. A., Holmén Larsson, J. M., Ekerhovd, E. & Hansson, G. C. Large scale identification of proteins, mucins, and their O-glycosylation in the endocervical mucus during the menstrual cycle. *Mol Cell Proteomics* **6**, 708-716, doi:10.1074/mcp.M600439-MCP200 (2007).
48 Barr, J. J. *et al.* Subdiffusive motion of bacteriophage in mucosal surfaces increases the frequency of bacterial encounters. *Proceedings of the National Academy of Sciences* **112**, 13675-13680, doi:doi:10.1073/pnas.1508355112 (2015).
49 Smith-Dupont, K. B. *et al.* Probing the potential of mucus permeability to signify preterm birth risk. *Scientific Reports* **7**, doi:10.1038/s41598-017-08057-z (2017).
50 Lykke, M. R. *et al.* Vaginal, Cervical and Uterine pH in Women with Normal and Abnormal Vaginal Microbiota. *Pathogens* **10**, doi:10.3390/pathogens10020090 (2021).
51 Hackett, A., Trinick, R., Rose, K., Flanagan, B. & McNamara, P. Weakly acidic pH reduces inflammatory cytokine expression in airway epithelial cells. *Respiratory research* **17**, 82 (2016).
52 McKinnon, K. E. *et al.* Development of human ectocervical tissue models with physiologic endocrine and paracrine signaling†. *Biol Reprod* **103**, 497-507, doi:10.1093/biolre/ioaa068 (2020).
53 Papanicolaou, G. Mucus test. *The Anatomical Record* **91**, 293 (1945).
54 Barrett, K. E., Boitano, S., Barman, S. M. & Brooks, H. L. Ganong's review of medical physiology twenty. (2010).

55 Straub, R. H. The Complex Role of Estrogens in Inflammation. *Endocrine Reviews* **28**, 521-574, doi:10.1210/er.2007-0001 (2007).

56 Zeng, R., Li, X. & Gorodeski, G. I. Estrogen Abrogates Transcervical Tight Junctional Resistance by Acceleration of Occludin Modulation. *The Journal of Clinical Endocrinology & Metabolism* **89**, 5145-5155, doi:10.1210/jc.2004-0823 (2004).

57 Anahtar, M. N., Gootenberg, D. B., Mitchell, C. M. & Kwon, D. S. Cervicovaginal Microbiota and Reproductive Health: The Virtue of Simplicity. *Cell Host Microbe* **23**, 159-168, doi:10.1016/j.chom.2018.01.013 (2018).

58 Morrill, S., Gilbert, N. M. & Lewis, A. L. Gardnerella vaginalis as a Cause of Bacterial Vaginosis: Appraisal of the Evidence From in vivo Models. *Frontiers in Cellular and Infection Microbiology* **10**, doi:10.3389/fcimb.2020.00168 (2020).

59 Ravel, J. *et al.* Daily temporal dynamics of vaginal microbiota before, during and after episodes of bacterial vaginosis. *Microbiome* **1**, 29, doi:10.1186/2049-2618-1-29 (2013).

60 Fernando, L. *Sperm intrauterine fluid interaction test - A new sperm function test*, (2007).

61 Agarwal, K. *et al.* Resident microbes shape the vaginal epithelial glycan landscape. *medRxiv*, 2022.2002.2023.22271417, doi:10.1101/2022.02.23.22271417 (2022).

62 Arnold, J. T. Endometrial stromal cells regulate epithelial cell growth in vitro: a new co-culture model. **16**, 836-845, doi:10.1093/humrep/16.5.836 (2001).

63 Chumduri, C. *et al.* Transition of Wnt signaling microenvironment delineates the squamo-columnar junction and emergence of squamous metaplasia of the cervix. *bioRxiv*, 443770, doi:10.1101/443770 (2018).

64 Kasendra, M. *et al.* Development of a primary human Small Intestine-on-a-Chip using biopsy-derived organoids. *Scientific reports* **8**, 1-14 (2018).

65 Ingber, D. E. Human organs-on-chips for disease modelling, drug development and personalized medicine. *Nature Reviews Genetics*, doi:10.1038/s41576-022-00466-9 (2022).

66 McGuckin, M. A., Lindén, S. K., Sutton, P. & Florin, T. H. Mucin dynamics and enteric pathogens. *Nature Reviews Microbiology* **9**, 265-278 (2011).

67 Kobayashi, M., Lee, H., Nakayama, J. & Fukuda, M. Roles of gastric mucin-type O-glycans in the pathogenesis of Helicobacter pylori infection. *Glycobiology* **19**, 453-461 (2009).

68 González-Rodríguez, I. *et al.* Role of extracellular transaldolase from Bifidobacterium bifidum in mucin adhesion and aggregation. *Applied and environmental microbiology* **78**, 3992-3998 (2012).

69 Ng, K. Y. B., Mingels, R., Morgan, H., Macklon, N. & Cheong, Y. In vivo oxygen, temperature and pH dynamics in the female reproductive tract and their importance in human conception: a systematic review. *Hum Reprod Update* **24**, 15-34, doi:10.1093/humupd/dmx028 (2018).

70 Check, J., Nowroozi, K., Wu, C., Liss, J. & Dietterich, C. The use of pelvic sonography and serum extradiol and progesterone assays in diagnosis and treatment of cervical factor. *Infertility* **9**, 247-256 (1986).

71 Chen, C. *et al.* The microbiota continuum along the female reproductive tract and its relation to uterine-related diseases. *Nat Commun* **8**, 875, doi:10.1038/s41467-017-00901-0 (2017).

72 Manhanzva, M. T. *et al.* Inflammatory and antimicrobial properties differ between vaginal Lactobacillus isolates from South African women with non-optimal versus optimal microbiota. *Scientific Reports* **10**, 6196, doi:10.1038/s41598-020-62184-8 (2020).

73 Schroeder, H. A. *et al.* Herpes simplex virus-binding IgG traps HSV in human cervicovaginal mucus across the menstrual cycle and diverse vaginal microbial composition. *Mucosal immunology* **11**, 1477-1486 (2018).

74 McLoughlin, K., Schluter, J., Rakoff-Nahoum, S., Smith, A. L. & Foster, K. R. Host selection of microbiota via differential adhesion. *Cell host & microbe* **19**, 550-559 (2016).

75 Lewis, W. G., Robinson, L. S., Gilbert, N. M., Perry, J. C. & Lewis, A. L. Degradation, foraging, and depletion of mucus sialoglycans by the vagina-adapted Actinobacterium Gardnerella vaginalis. *Journal of Biological Chemistry* **288**, 12067-12079 (2013).

76 Cauci, S., McGregor, J., Thorsen, P., Grove, J. & Guaschino, S. Combination of vaginal pH with vaginal sialidase and prolidase activities for prediction of low birth weight and preterm birth. *American journal of obstetrics and gynecology* **192**, 489-496 (2005).

77 Pleckaityte, M., Janulaitiene, M., Lasickiene, R. & Zvirbliene, A. Genetic and biochemical diversity of Gardnerella vaginalis strains isolated from women with bacterial vaginosis. *FEMS Immunology & Medical Microbiology* **65**, 69-77 (2012).

78 Lai, S. K. *et al.* Human immunodeficiency virus type 1 is trapped by acidic but not by neutralized human cervicovaginal mucus. *Journal of virology* **83**, 11196-11200 (2009).

79 Lewis, A. L. & Lewis, W. G. Host sialoglycans and bacterial sialidases: a mucosal perspective. *Cellular microbiology* **14**, 1174-1182 (2012).

80 Tantengco, O. A. G., Richardson, L. S., Medina, P. M. B., Han, A. & Menon, R. Organ-on-chip of the cervical epithelial layer: A platform to study normal and pathological cellular remodeling of the cervix. *Faseb j* **35**, e21463, doi:10.1096/fj.202002590RRR (2021).

81 Huh, D. *et al.* Microfabrication of human organs-on-chips. *Nature Protocols* **8**, 2135-2157, doi:10.1038/nprot.2013.137 (2013).

82 Turco, M. Y. *et al.* Long-term, hormone-responsive organoid cultures of human endometrium in a chemically defined medium. *Nat Cell Biol* **19**, 568-577, doi:10.1038/ncb3516 (2017).

83 Phillips, C. L., Combs, S. B. & Pinnell, S. R. Effects of ascorbic acid on proliferation and collagen synthesis in relation to the donor age of human dermal fibroblasts. *J Invest Dermatol* **103**, 228-232, doi:10.1111/1523-1747.ep12393187 (1994).

84 Maoz, B. M. *et al.* A linked organ-on-chip model of the human neurovascular unit reveals the metabolic coupling of endothelial and neuronal cells. *Nature Biotechnology* **36**, 865-874, doi:10.1038/nbt.4226 (2018).

85 Xie, Y. *et al.* Glycan–protein cross-linking mass spectrometry reveals sialic acid-mediated protein networks on cell surfaces. *Chem. Sci.* **12**, 8767-8777, doi:10.1039/D1SC00814E (2021).

86 M.Furst, E. Particle tracking with Matlab.

87 Pelletier, V. & Kilfoil, M. Software Research Tools. *Kilfoil Lab* (2007).

88 Lieleg, O., Vladescu, I. & Ribbeck, K. Characterization of particle translocation through mucin hydrogels. *Biophysical journal* **98**, 1782-1789 (2010).

89 Metzler, R., Jeon, J.-H., Cherstvy, A. G. & Barkai, E. Anomalous diffusion models and their properties: non-stationarity, non-ergodicity, and ageing at the centenary of single particle tracking. *Physical Chemistry Chemical Physics* **16**, 24128-24164 (2014).

90 Metzler, R. & Klafter, J. The random walk's guide to anomalous diffusion: a fractional dynamics approach. *Physics reports* **339**, 1-77 (2000).

FIGURE LEGENDS

Fig 1. Development and characterization of human ecto-and endo-cervix chips. a. Photograph (left) and schematic cross-sectional view (right) of the dual channel microfluidic organ chip lined by human cervical epithelium interfaced across an ECM-coated porous membrane with human cervical fibroblasts. **b.** Phase-contrast microscopic view from above of a Cervix Chip lined by cervical epithelium and fibroblasts on the apical and basal sides of the chip porous membrane, respectively, on day 1 (left) as well as after 12 days of culture under continuous (middle) or periodic (right) flow (bar, 200µm). **c.** Side view, dark field images of living Cervix Chip hours after cell seeding day 0 (top) and after 7 days of differentiation (bottom). White arrow indicates light reflective mucus accumulating above the differentiated epithelium (bar, 1mm). **d.** Fluorescence microscopic side views of mucus layers in live Cervix Chip cultures stained with fluorescent wheat germ agglutinin (WGA) (green) on day 7 of differentiation under continuous (top) and periodic (bottom) flow regimens (bar, 1mm). **e.** Immunofluorescence microscopic view from above of the cervical epithelium stained for mucin 5B (green), F-actin (yellow), and nuclei with Hoechst (blue) (bar, 50 µm). **f.** Immunofluorescence microscopic vertical cross sectional view of the chip showing the cervical epithelium stained for MUC5B (green) overlaying the porous membrane, the underlying layer of fibroblasts stained for vimentin (yellow), and Hoechst-stained nuclei (blue) (bar, 20 µm). **g.** Quantification of the total mucin content produced by Cervix Chips cultured under continuous (black symbols) or periodic (white symbols) flow at days 0 and 7 of differentiation measured using an Alcian Blue assay. **h.** Cytokine proteins in effluents of Cervix Chips cultured under continuous (gray bars) or periodic flow (white bars) on day 0 versus 7 of differentiation. **i.** RNAseq analysis of genes expressed in cervical epithelial cells from African American, Hispanic, and Caucasian donors differentiated in static Transwells or Cervix Chips under periodic or continuous flow for 12 days. Expression levels of the signature genes associated with the endo- and ecto-cervical epithelial cells[44] were compared using Z-scores calculated per donor across samples for the

three flow regimens, emphasizing common trends among samples of different background (colors represent gene expression levels). Data represent the mean ± s.e.m.; n=3-5 (**g**), 4-5 (**h**), and 3 (**i**) biological chip replicates; ** P ≤ 0.05, *** P<0.001, **** P<0.0001*.

Fig 2. Recapitulation of the compositional and biophysical properties of cervical mucus. a. Glycomic analysis showing representative O- and N-glycan profiles of mucus produced by cervical epithelial cells cultured in Transwells or Cervix Chips exposed to periodic or continuous flow compared to a clinical sample of human mucus. The compound peaks are color coded to show the glycan subtypes and numbered to represent the glycan molecules structures: (#_#_#_#) format represents number of core structure type 1_number of core structure type 2_number of glycan subtype 1_number of glycan subtype 2. **b**. Tables showing the most abundant O- and N-glycan subtypes observed in the mucus profiles of human clinical samples compared with Cervix Chips exposed to periodic or continuous flow (combined peaks) versus Transwell cultures. **c.** Graph showing diffusion constant measured in mucus within the Cervix Chip developed using periodic flow regimen and in Transwells compared to human clinical mucus. Data represent the mean ± s.e.m.; n=3-9 biological chip replicates; ** P ≤ 0.05.*

Fig. 3. Recapitulation of cervical mucus responses to physiological pH and sex hormones in the Cervix Chip. a. Left) Dark field (top) and fluorescence (bottom) side views of unlabeled and WGA-stained mucus in live Cervix Chips cultured at pH 7.1 compared to pH 5.4. Double headed dashed arrows show mucus thickness (bar, 200 µm). Right) Graph showing changes in the % of area containing WGA-stained mucus in the apical epithelium channel. **b.** Graph showing fold change in expression of cervical epithelial genes encoding mucin 4 (MUC4) and secretory leukocyte peptidase inhibition (SLPI) in Cervix Chips cultured at pH 7.1 and pH 5.4 measured using real-time PCR. **c.** Graph showing TNF-α level in Cervix Chips cultured at pH 5.4 compared to 7.1. **d.** Fluorescence side view micrographs of WGA-stained mucus in live cervix chips showing increased mucus layer thickness when cultured with high estrogen (ovulatory, 5nM E2+0nM P4) compared to high progesterone (non-ovulatory, 0.5nM E2+50nM P4) levels

(double headed arrows show mucus thickness; bar, 200 µm). **e.** Total mucus content (mucus thickness x immunofluorescence intensity) measured in live Cervix Chips cultured under different hormonal conditions shown in **d**. **f.** Cervix Chip mucus diffusion constant measured on-chip under high estrogen compared to high progesterone hormone levels. **g.** Bright field images of the mucus Fern Test collected from Cervix Chips under ovulatory (high estrogen) compared to non-ovulatory (high progesterone) hormone conditions (bar, 200 µm). **h.** Cytokine secretion levels measured in cervix chips under high estrogen (ovulatory, 5nM E2+0nM P4) compared to high progesterone (non-ovulatory, 0.5nM E2+50nM P4) hormone conditions. **i.** Changes in tissue barrier function in the Cervix Chip measured using TEER under high estrogen versus high progesterone hormone levels using the TEER sensor-integrated chip (red arrow indicate start of hormone treatment). **j.** Dynamic changes in the epithelial barrier function when hormones are changed from ovulatory to non-ovulatory conditions at day 6 of differentiation (red arrow indicates time that hormone treatment switches from ovulatory to non-ovulatory conditions. Data represent the mean ± s.e.m.; n=5 (**a**), 3-5 (**b**), 4-5 (**c**), 6 (**e**), 3 (**f**), 3-6 (**h**), and 3 (**i,j**) biological chip replicates; ** P ≤ 0.05, ** P<0.01, *** P<0.001, **** P<0.0001*.

Fig 4. Modeling cervical epithelial host interactions with *L. crispatus* and *G. vaginalis* consortia in Cervix Chips. a. Phase-contrast (Top) and immunofluorescence (bottom) microscopic views from above of the Cervix Chip co-cultured with *L. crispatus* consortia. Top) Phase-contrast microscopic view (left) and higher magnification image (right) of live chip cervical epithelium colonized with *L. crispatus* bacteria. Bottom) Immunofluorescence micrographs of cervical epithelium stained for mucin 5B (green) (left), nuclei with Hoechst (blue) (middle) and the overlay image (right) (Black and white arrows show *L. crispatus* bacteria colonized on-chip; bar, 50 µm). **b.** Immunofluorescence micrographs of cervical epithelium stained for F-actin (yellow) and nuclei with Hoechst (blue) in Cervix Chip co-cultured with no bacteria (left), *L. crispatus* (middle) and *G. vaginalis* (right) (White arrows show *G. vaginalis* bacteria colonized on the epithelium; bar, 50 µm). **c.** Enumeration of the total non-adherent (Effluent; white bar)

and adherent (Digest; grey bar) bacteria in the Cervix Chip during and at the end of co-culture, respectively, with the *L. crispatus* or *G. vaginalis* consortia compared to the initial inoculum in the Cervix Chip. **d.** Graph showing percentage change in the viability of cervical epithelial cells after 72 hours of co-culture with *L. crispatus* or *G. vaginalis* consortia in the Cervix Chip compared to control chip without bacteria. **e.** Graph showing fold change in the cervix Chip barrier permeability during co-culture time with *L. crispatus* or *G. vaginalis* consortia compared to non-inoculated, control chip as measured by apparent permeability (P_{app}). **f.** Heat map showing Cervix Chip epithelium innate immune response to *L. crispatus* or *G. vaginalis* consortia at 72 hours post inoculation quantified by levels of IL-1α, IL1-β, TNF-α, IL-6, IL-8 in the epithelial channel effluents. The color-coded scale represents LOG10 fold change in cytokine levels over control chip. Data represent the mean ± s.e.m.; n=7-14 (**c**), 3-6 (**d**), 7-14 (**e**), and 10-14 (f); biological chip replicates; ** P ≤ 0.05, ** P<0.01, *** P<0.001, **** P<0.0001*.

Fig 5. Modelling modulation of cervical mucus with *L. crispatus* and *G. vaginalis* consortia on Cervix Chip. a. Fluorescence side view micrographs of WGA-stained mucus in live Cervix Chips co-cultured with *L. crispatus* (middle) or *G. vaginalis* (bottom) compared to control chip (top) without bacteria (white dashed line indicates porous membrane; bar, 200µm). **b.** Total mucus content (mucus thickness x immunofluorescence intensity) measured in live Cervix Chips cultured with *L. crispatus* or *G. vaginalis* compared to nob-inoculated control chip. **c.** Graph showing the spatial distribution of the live mucus immunofluorescence intensity along the width of the epithelial channel in the Cervix Chip co-cultured with *L. crispatus* or *G. vaginalis* consortia compared to control chip. **d.** Bright field images of the mucus Fern Test collected from Cervix Chips co-cultured with *L. crispatus* or *G. vaginalis* consortia compared to control chip without bacteria (bar, 200 µm). **e,f.** Graphs showing fold change in the live mucus diffusion constant (**e**) and diffusion exponent (**f**) in Cervix Chips co-culture with *L. crispatus*, *G. vaginalis*, or no bacteria. **g.** Pie charts representing the relative abundances of O-glycan types in the Cervix Chip mucus after 72 hours of co-culture with *L. crispatus* or *G. vaginalis* consortia compared to

control chip without bacteria quantified using nanoLC-QTOF MS/MS. **h.** Relative abundance of undecorated and sialylated O-glycans in the Cervix Chip mucus collected after 72 hours of co-culture with *L. crispatus* or *G. vaginalis* consortia compared to control chip. Data represent the mean ± s.e.m.; n=3 (**b**), 6-7 (**e,f**), and 3-6 (**h**) biological chip replicates; ** P ≤ 0.05, ** P<0.01, *** P<0.001, **** P<0.0001*.

Supplementary Figures legends:

Supplementary Fig. S1. Characterization of the human Cervix Chip. a. Immunofluorescence micrographs of the cervical epithelial cells in 2D culture stained for cytokeratin 14 (CK14, green) (left) and cytokeratin 7 (CK7, magenta) (right) showing a mixture of primary human endo- and ecto-cervical epithelial cells, respectively (bar, 100 µm)**. b.** Immunofluorescence microscopic vertical cross sectional views of the chip showing the cervical epithelium stained for cytokeratin 18 (CK18, white) (left), estrogen receptor (ER, red) (middle), progesterone receptor (PR, green) (right), and Hoechst-stained nuclei (blue) (bar, 20 µm). **c.** Quantification of the change in the epithelial cells growth and differentiation in Cervix Chip measured by left) percentage change in the number of cells stained for Ki67, and right) surface area (μm^2) stained for mucin 5B per cell in the epithelium throughout the culture time. **d.** Graph showing fold change in expression of cervical epithelial genes encoding mucin 4 (MUC4), Mucin 5B (MUC%B), and secretory leukocyte peptidase inhibition (SLPI) in Cervix Chip and Transwell compared to 2D culture. **e.** Graph showing real-time changes in the Cervix Chip transepithelial electrical resistance (TEER) measured using custom made Organ Chip with integrated electrodes compared to Transwell culture measured using IVUM2 (red arrow indicates start of differentiation in culture). **f.** Gene set scoring analysis showing relative ratio of the upregulated epithelial genes relative to the signature ectocervical genes[44] in Cervix Chip cell developed using periodic and continuous flow regimen and Transwell culture for donors from African American, Hispanic, and Caucasian background quantified

using bulk RNAseq analysis of cervical epithelial cells. **g.** Left) Phase-contrast and (middle) immunofluorescence microscopic view cervical epithelium in a Transwell (top) and Cervix Chip (bottom) culture, and right) Immunofluorescence microscopic view of fibroblast stroma stained for F-actin (yellow) (bar 50 µm). **h.** Non-invasive single particle tracking method used to quantify mucus diffusion properties in live chips. Left) An overlay of phase contrast and fluorescence images of randomly dispersed 1µM fluorescent particles (red) within fluorescent WGA-stained mucus (green) on-chip (inset, tracked particles in a single frame are highlighted). Right) Overlay of side view image of mucus overlying the epithelium (red) showing randomly dispersed microparticles (red) (white dashed line indicates porous membrane; double headed arrow indicates the mucus thickness) (bar, 100 µm). Data represent the mean ± s.e.m.; n=3 (**b**), 3 (**c**), 3-8 (**d**), and 3 (**e**) biological chip replicates; ** *P ≤ 0.01, *** P<0.001, **** P<0.0001*.

Supplementary Fig. S2. **Characterization of Cervix Chip responses to physiological pH and sex hormones in the Cervix Chip. a.** Graph showing changes in the pH of the Cervix Chip inflow and outflow media when cultured at pH 7.1 compared to pH 5.4. **b.** Quantification of permeability in Cervix Chip cultured under at pH 7.1 compared to pH 5.4 as measured by apparent permeability (P_{app}). **c.** Quantification of total mucin content produced by each cell in Cervix Chip cultured at pH 7.1 compared to pH 5.4 using an Alcian Blue assay. **d.** Graph showing fold change in the expression of cervical epithelial genes encoding mucin 5B (MUC5B) and asparaginase and isoaspartyl peptidase (ASRGL) in Cervix Chip cultured at pH 7.1 and pH 5.4 using real-time PCR. **e.** Quantification of total mucin content produced by Cervix Chip cultured with high estrogen (5nM E2+0nM P4) compared to high progesterone (0.5nM E2+50nM P4) hormone levels using Alcian Blue assay. **f.** Graph showing change in expression level ratio of cervical genes encoding mucin 5B (MUC5B) and mucin 5AC (MUC5AC) in the Cervix Chips culture with high estrogen (5nM E2+0nM P4) compared to high progesterone (0.5nM E2+50nM P4) hormone levels. **g.** Changes in the abundance of O- and N-glycan compounds in the mucus collected

from Cervix Chip cultured with high estrogen (HE, 5nM E2+0nM P4) compared to high progesterone (HP, 0.5nM E2+50nM P4) levels detected using nanoLC-QTOF MS/MS glycomic analysis (Upward and downward arrows indicate increase and decrease, respectively, in the relative abundance of glycans in the HP compared to HE chips). Data represent the mean ± s.e.m.; n=4 (**a**), 5 (**b**), 3 (**c**), 4-5 (**d**), 3 (**e**), 5 (**f**), and 6 (**g**) biological chip replicates; ** $P \leq 0.05$,* n.s., not significant.

Supplementary Fig. S3. **a.** Graph showing changes in the pH of the Cervix Chip epithelium effluents co-cultured in the absence or presence of *L. crispatus* or *G. vaginalis* consortia at 72 hours post inoculation compared to control basal channel. **b.** Quantification of total mucin content in the Cervix Chip effluents co-cultured with *L. crispatus* or *G. vaginalis* consortia compared to control chip without bacteria using an Alcian Blue assay. Data represent the mean ± s.e.m.; n=6-7 (**a**), and 3 (**b**) biological chip replicates; n.s., not significant.

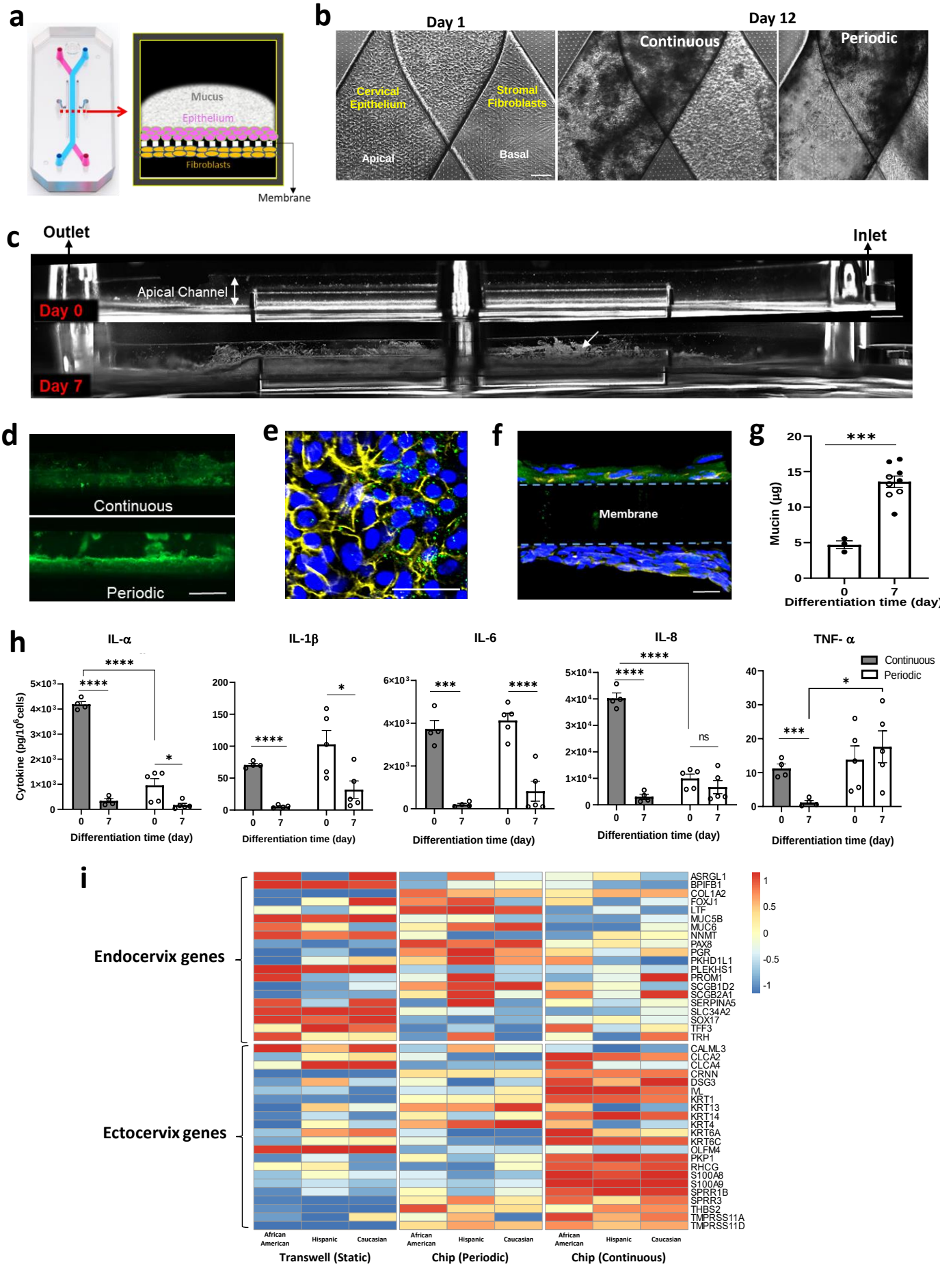

Fig. 1

a

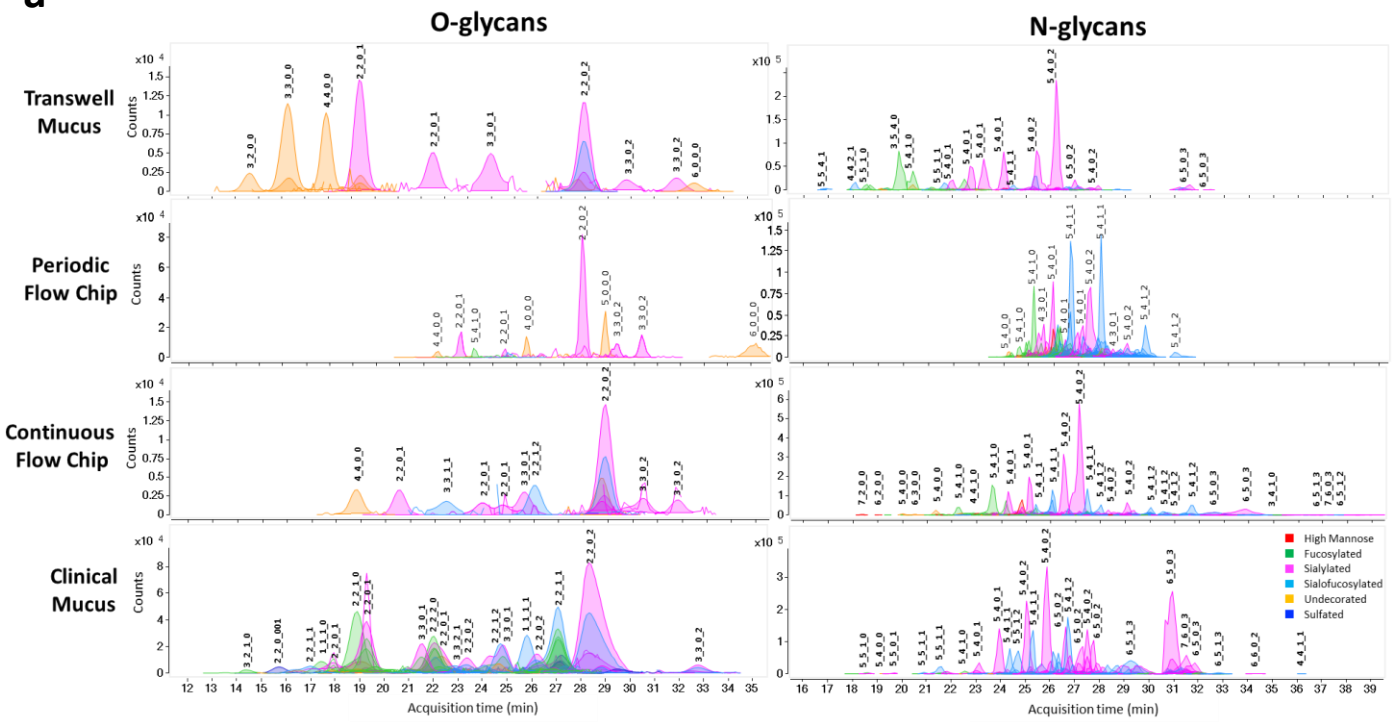

b

O-glycans			
Class (Compound | Retention time)	Human Clinical Mucus	Combined Chip Mucus	Transwell Mucus
Sialylated (2_2_0_2|28.2)	×	×	×
Fucosylated (2_2_1_0|18.9)	×		
Sialofucosylated (2_2_1_1|27.0)	×		
Sialylated (2_2_0_1|19.3)	×	×	×
Sialofucosylated (1_1_1_1|25.8)	×		
Fucosylated (2_2_2_0|21.9)	×		
Sialylated (3_3_0_1|21.6)	×		
Sialofucosylated (2_2_1_2|24.7)	×	×	
Sialylated (3_3_0_1|24.8)	×	×	×
Sialylated (2_2_0_2|26.1)	×		
Sialylated (3_3_0_2|32.8)	×	×	×

N-glycans			
Class (Compound | Retention time)	Human Clinical Mucus	Combined Chips Mucus	Transwell Mucus
Sialylated (6_5_0_3|30.9)	×	×	×
Sialylated (5_4_0_2|25.9)	×	×	×
Sialylated (5_4_0_2|25.1)	×	×	×
Sialofucosylated (5_4_1_2|26.7)	×	×	×
Sialylated (5_4_0_1|24.0)	×	×	×
Sialofucosylated (6_5_1_3|29.3)	×		
Sialylated (7_6_0_3|31.5)	×		
Sialylated (5_4_0_2|27.5)	×	×	×
Sialylated (6_5_0_2|26.6)	×		
Sialofucosylated (5_4_1_1|25.3)	×	×	×
Sialylated (5_4_0_1|23.1)	×	×	×
Fucosylated (5_4_1_0|22.6)	×	×	×

c

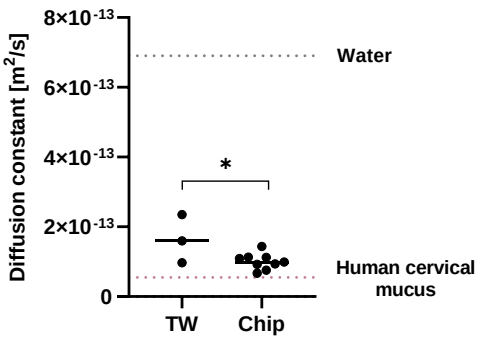

Fig. 2

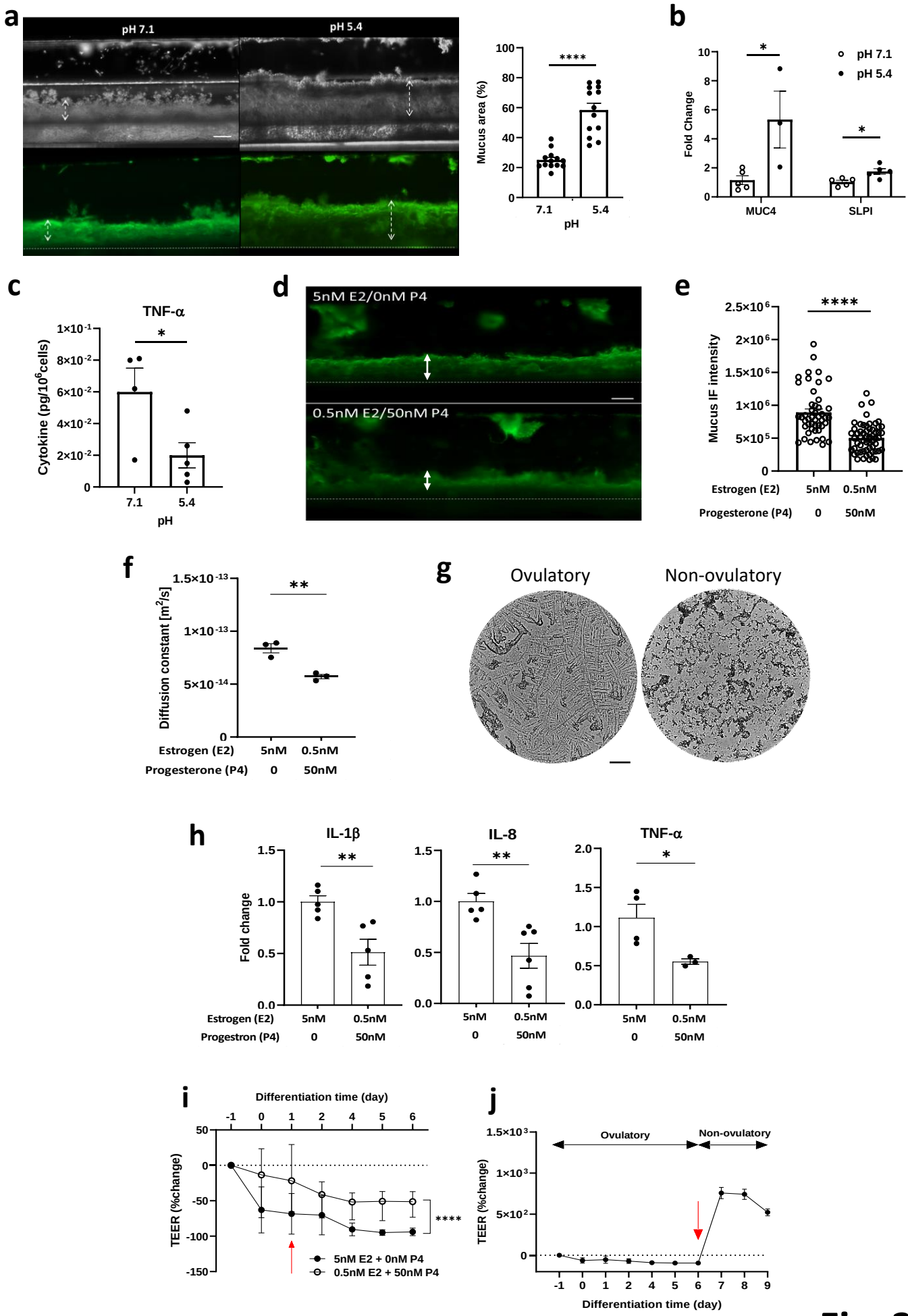

Fig. 3

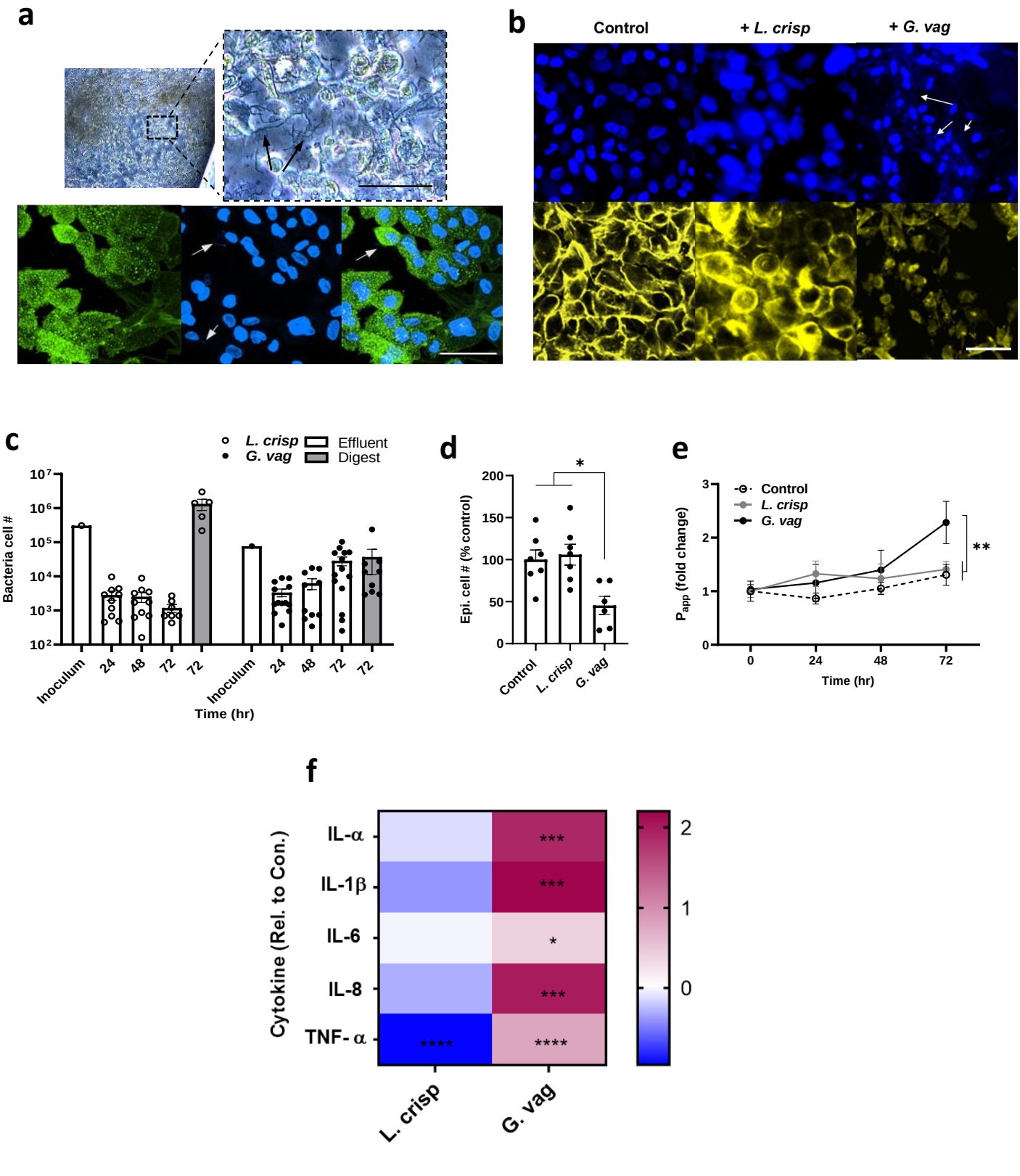

Fig. 4

Fig. 5

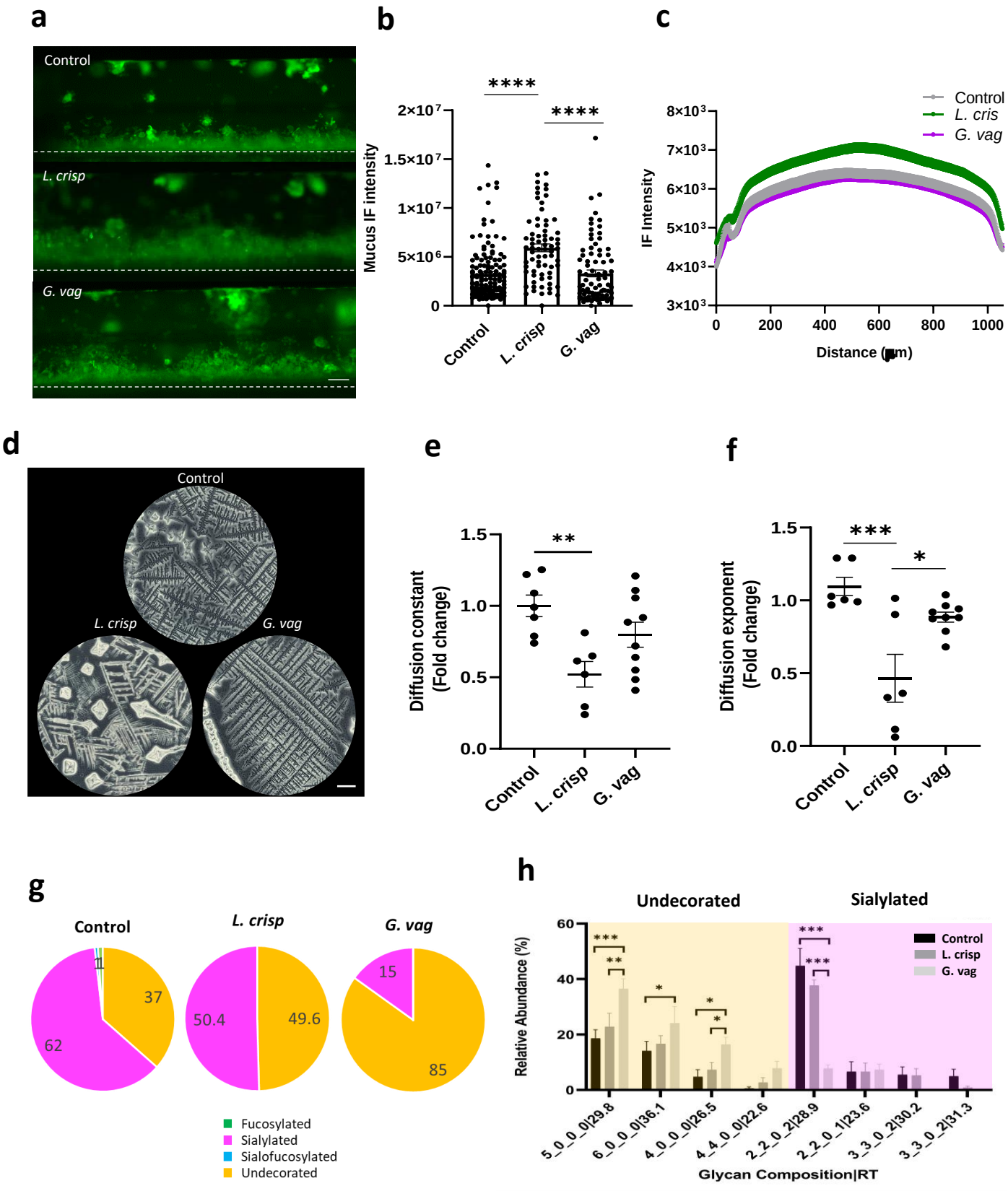

Fig. 5

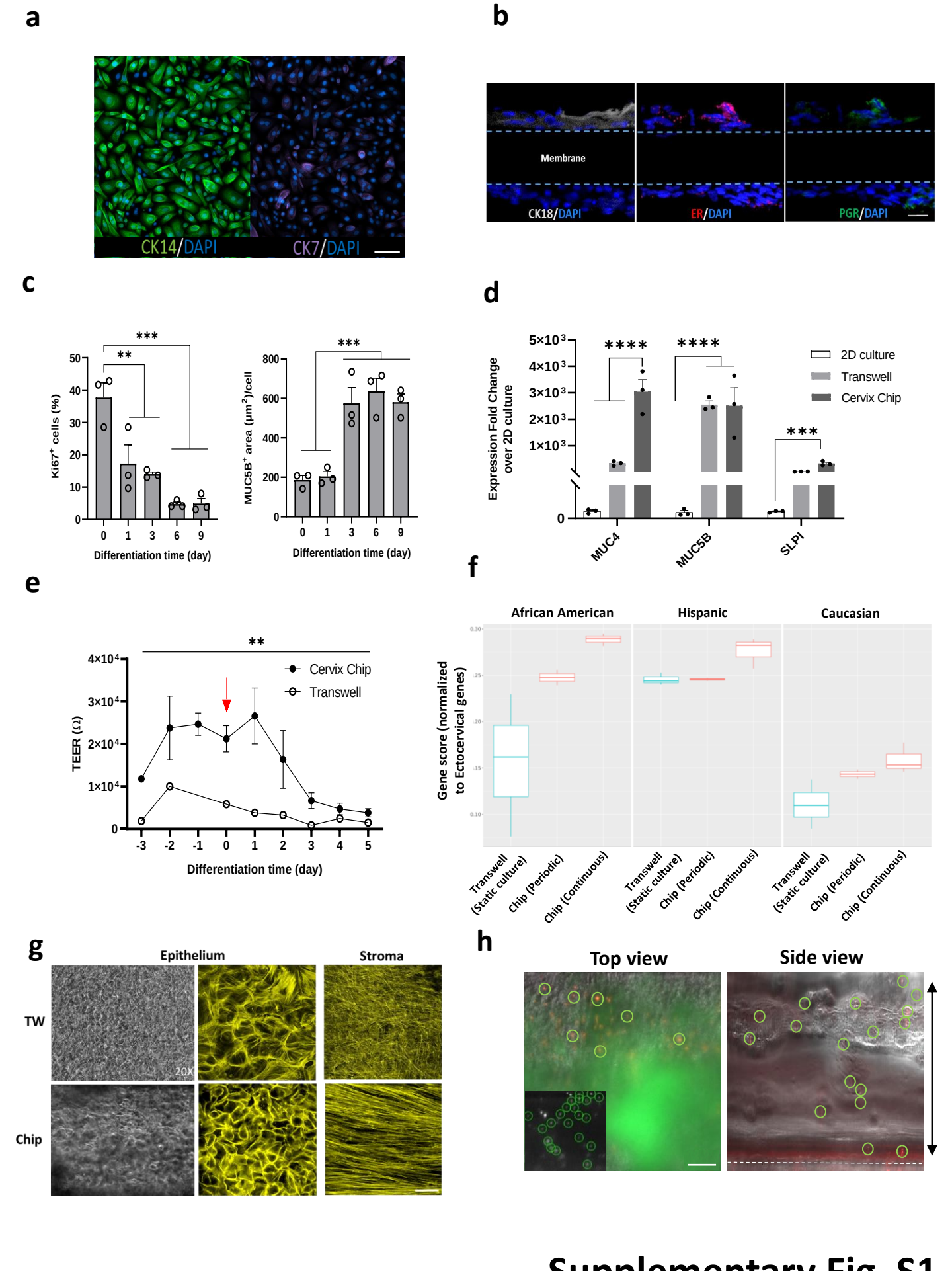

Supplementary Fig. S1

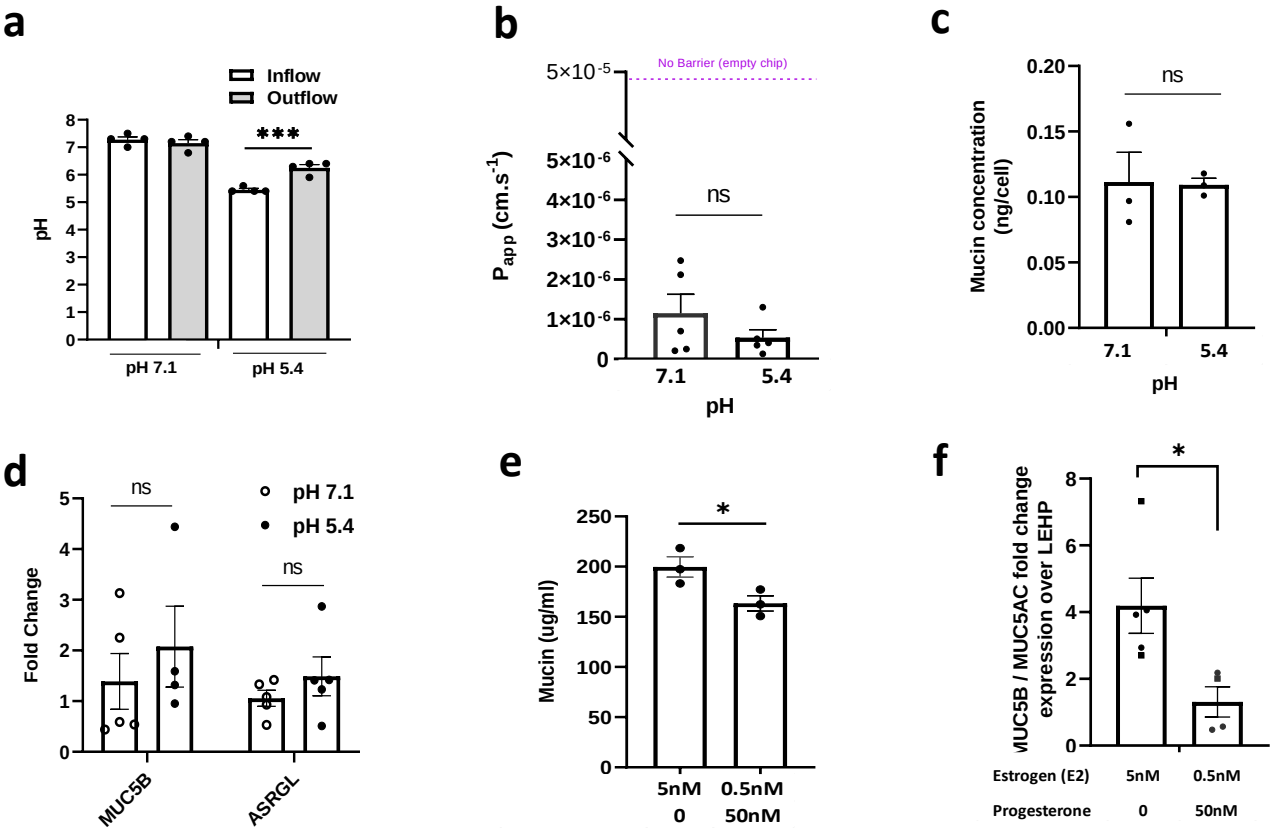

g

Class (Compound|Retention time)	Human Clinical Mucus	Cervix Chip HE	Cervix Chip HP
O-glycans			
Sialylated (2_2_0_2|28.2)	×	×	↓
Fucosylated (2_2_1_0|18.9)	×		
Sialylated and fucosylated (2_2_1_1|27.0)	×		
Sialylated (2_2_0_1|19.3)	×	×	↑
Sialylated and fucosylated (1_1_1_1|25.8)	×		
Fucosylated (2_2_2_0|21.9)	×		
Sialylated (3_3_0_1|21.6)	×		
Sialylated and fucosylated (2_2_1_2|24.7)	×	×	↓
Sialylated (3_3_0_2|24.8)	×	×	
Sialylated (2_2_0_2|26.1)	×		×
N-glycans			
Sialylated (6_5_0_3|30.9)	×	×	↓
Sialylated (5_4_0_2|25.9)	×	×	↓
Sialylated (5_4_0_2|25.1)	×	×	↓
Sialylated and fucosylated (5_4_1_2|26.7)	×	×	↓
Sialylated (5_4_0_1|24.0)	×	×	↓
Sialylated and fucosylated (6_5_1_3|29.3)	×		
Sialylated (7_6_0_3|31.5)	×		
Sialylated (5_4_0_2|27.5)	×	×	↓
Sialylated (6_5_0_2|26.6)	×		
Sialylated and fucosylated (5_4_1_1|25.3)	×	×	×
Sialylated (5_4_0_1|23.1)	×	×	↓
Fucosylated (5_4_1_0|22.6)	×	×	↓

Supplementary Fig. S2

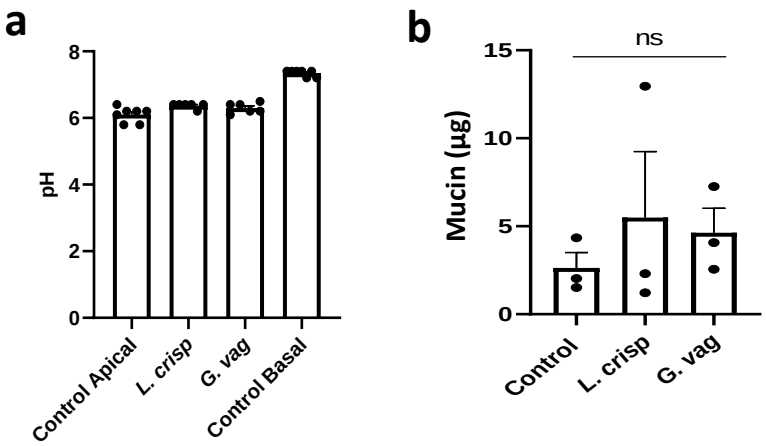

Supplementary Fig. S3